HHS Public Access

Author manuscript

Cell Metab. Author manuscript; available in PMC 2020 November 05.

Published in final edited form as:

Cell Metab. 2019 November 05; 30(5): 890–902.e8. doi:10.1016/j.cmet.2019.08.012.

Mediation of the acute stress response by the skeleton

Julian Meyer Berger[1,2], **Parminder Singh**[3], **Lori Khrimian**[1], **Donald A. Morgan**[4], **Subrata Chowdhury**[1], **Emilio Arteaga-Solis**[1,5], **Tamas L. Horvath**[6], **Ana I. Domingos**[7], **Anna L. Marsland**[8], **Vijay Kumal Yadav**[1,3], **Kamal Rahmouni**[4], **Xiao-Bing Gao**[6], **Gerard Karsenty**[1,*]

[1]Department of Genetics and Development, Columbia University Irving Medical Center, New York, NY 10032, USA.

[2]Program in Microbiology, Immunology and Infection, Columbia University Irving Medical Center, New York, NY 10032, USA.

[3]Metabolic Research Laboratory, National Institute of Immunology, Aruna Asaf Ali Marg, New Delhi 110067, India.

[4]Department of Pharmacology, University of Iowa and Veteran Health Care System, Iowa City, IA 52242, USA.

[5]Division of Pediatric Pulmonary, Department of Pediatrics, Columbia University Irving Medical Center, New York, NY 10032, USA.

[6]Program in Integrative Cell Signaling and Neurobiology of Metabolism, Department of Comparative Medicine, Yale University School of Medicine, New Haven, CT USA.

[7]Department of Physiology, Anatomy and Genetics, University of Oxford, Oxford, UK.

[8]Department of Psychology, University of Pittsburgh, Pittsburgh, PA 15260, USA

Summary

We hypothesized that bone evolved, in part, to enhance the ability of bony vertebrates to escape danger in the wild. In support of this notion we show here that a bone-derived signal is necessary to develop an acute stress response (ASR). Indeed, exposure to various types of stressors in mice, rats (rodents) and humans leads to a rapid and selective surge of circulating bioactive osteocalcin because stressors favor the uptake by osteoblasts of glutamate, which prevents inactivation of osteocalcin prior to its secretion. Osteocalcin permits manifestations of the ASR to unfold by signaling in post-synaptic parasympathetic neurons to inhibit their activity, thereby leaving the

[*]Lead Contact, please address correspondence to: Gerard Karsenty, Department of Genetics and Development, 701 W. 168th Street, Room 1602A HHSC, New York, NY, 10032, USA. Phone: 212.305.4011; Fax: 212.923.2090; gk2172@cumc.columbia.edu.

Author contributions

J.M.B. and G.K. conceived of the study. J.M.B., V.K.Y., K.R., X.B.G., and G.K. designed experiments. J.M.B., V.K.Y., P.S., L.K., E.A.S., S.C., D.M., K.R., and X.B.G. performed experiments. T.L.H., A.I.D., and A.L.M. contributed reagents. J.M.B., K.R. and G.K. analyzed data and wrote the manuscript.

Declaration of Interests

The authors declare no competing financial interests.

sympathetic tone unopposed. Like wild-type animals, adrenalectomized rodents and adrenal-insufficient patients can develop an ASR, and genetic studies suggest that this is due to their high circulating osteocalcin levels. We propose that osteocalcin defines a bony vertebrate specific endocrine mediation of the ASR.

Graphical Abstract

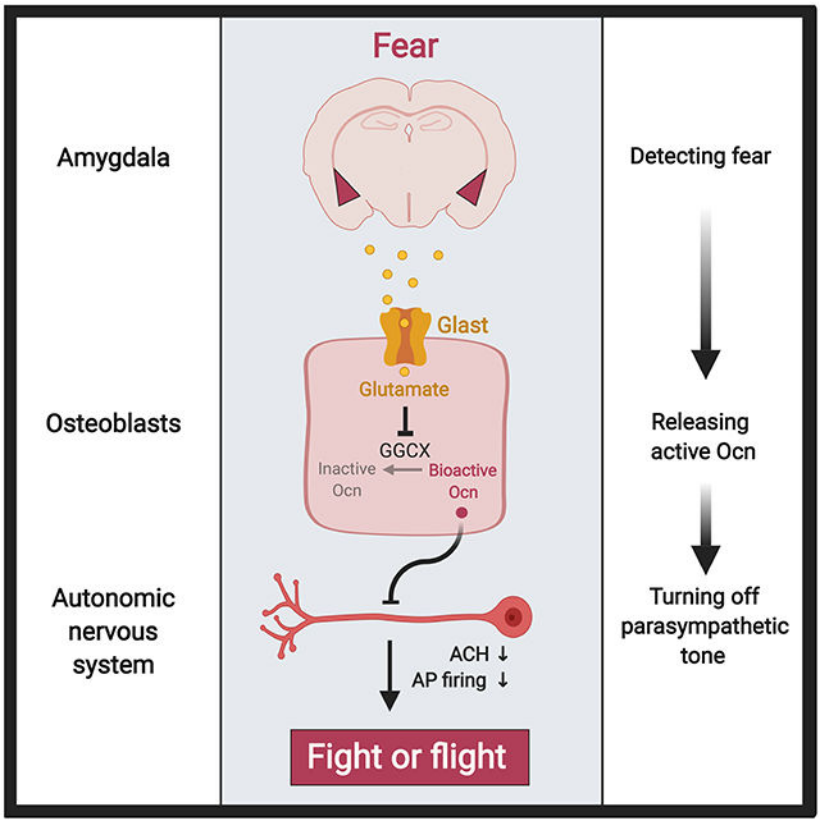

eTOC

During the acute stress response in bony vertebrates, a brain-derived signal increases glutamate uptake into osteoblasts, producing a surge in circulating osteocalcin. Once released, osteocalcin suppresses the parasympathetic nervous system, enabling the stress response.

Introduction

The endocrine functions of bone raise the question of why an organ viewed as a scaffold is also an endocrine organ. A possible answer to this question arises by considering bone physiology in an evolutionary context. Through its structural properties bone protects internal organs in the event of a trauma and allows animals to move and escape danger (Romer, 1933). Bone also mediates hearing, which is a means of detecting danger. A similar purpose in the context of danger may be ascribed to several physiological processes enhanced by the bone-derived hormone osteocalcin. Memory is needed in the wild to recall where food and/or predators are; the ability to increase exercise capacity is an absolute

necessity for animals attempting to escape danger; and circulating testosterone levels rise in the event of danger (Frankel and Ryan, 1981; Karsenty and Olson, 2016; Mera et al., 2016; Yuen et al., 2009). From this vantage point, one could argue that the classical and endocrine functions of bone concur to equip bony vertebrates with a tool to escape danger. If this interpretation is, at least in part, correct, bone should regulate other physiological functions activated in the presence of danger.

The acute stress response (ASR) is an evolutionarily conserved physiological process that aims to maintain or restore homeostasis in animals facing an immediate danger. Such danger produces an increase in temperature and energy expenditure, higher heart rate, and faster respiration, among other manifestations (McEwen, 1998; Sapolsky et al., 2000; Ulrich-Lai and Herman, 2009). The sympathetic nervous system that releases catecholamine into peripheral organs is considered to be the ultimate mediator of the ASR in vertebrates (Axelrod and Reisine, 1984; Ulrich-Lai and Herman, 2009). In addition, circulating glucocorticoid hormones surge during an ASR, suggesting that an endocrine mediation of the ASR may exist. As steroids, glucocorticoid hormones act mainly, albeit not only, at the transcriptional level and need hours to regulate physiological processes (Tsai and O'Malley, 1994), something that seems inconsistent with the need for an immediate response. Although this certainly does not rule out that glucocorticoid hormones may be implicated in some capacity in the ASR, it suggests the possibility that other hormones, possibly peptide ones, could mediate the ASR. This is why, in considering that an original purpose of bone was to escape danger, we asked whether bone-derived hormones contribute to the ASR in bony vertebrates.

Addressing the aforementioned question revealed that osteocalcin is necessary to develop an ASR. Osteocalcin circulating levels surge within minutes in mice exposed to stressors. This effect of stressors on bone is restricted to osteocalcin, independent of corticosterone and catecholamine signaling, but requires that osteoblasts take up glutamate to enhance the release of bioactive osteocalcin. Osteocalcin is necessary for the development of several key manifestations of an ASR by signaling through its receptor Gprc6a in post-ganglionic parasympathetic neurons to inhibit cholinergic activity. Remarkably, adrenalectomized rodents and patients with adrenal insufficiency can still mount a normal ASR. Genetic experiments indicate that this is due to a doubling of circulating osteocalcin in these animals. These results identify bone as a stress organ and osteocalcin as a stress hormone.

Results

Stressors trigger a rapid surge of circulating bioactive osteocalcin in rodents and humans

Testing whether any protein made in bone is affected during the acute stress response (ASR) revealed that circulating levels of undercarboxylated, i.e., bioactive, osteocalcin rose by 50% after a 45-minute-long restraint and by 150% 15 minutes after electric foot shocks in 2- to 6-month-old mice, in either sex, in two different genetic backgrounds, and at two different times of day (Figures 1A-E). Circulating bioactive osteocalcin levels also rose in rats after restraint and in humans submitted to a public speaking and cross-examination stress that increased heart rate and blood pressure (Patterson-Buckendahl et al., 1995; Prather et al., 2009) (Figures 1F-G). This effect of stressors on bone seen in rodents and humans is

restricted to osteocalcin, as circulating levels of other bone-derived hormones and synthesis of Type I collagen, the most abundant protein of the bone matrix, are unaffected in stressor-exposed mice (Figures S1A-C).

As a third stressor we also used 2,4,5-trimethyl thiazoline (TMT), a component of fox urine, because it triggers a rapid, innate and centrally controlled fear reaction in the mouse (Kim et al., 2016; Kobayakawa et al., 2007; Kondoh et al., 2016; Root et al., 2014). TMT induced a rise in circulating bioactive osteocalcin that began before that of corticosterone, reached its peak at 2.5 minutes and remained steady for at least 3 hours. In contrast, urine from a non-predator animal used as a negative control did not affect circulating bioactive osteocalcin (Figures 1H-I). The effect of TMT on circulating bioactive osteocalcin prompted us to assess through a chemogenetic designer receptor exclusively activated by designer drugs (DREADD) approach (Zhu and Roth, 2014) whether stressors signal in the brain to induce a rise in circulating bioactive osteocalcin. Adeno-associated virus (AAV) encoding the inhibitory DREADD hM4Di was injected into the baso-lateral amygdala (BLA), a brain region proposed to be a fear center in the murine brain, involved in TMT neuronal relays and selectively labeled by viral retrograde tracing from the femur (Denes et al., 2005; Fadok et al., 2009; Johansen et al., 2011; Muller and Fendt, 2006; Terburg et al., 2018; Tye et al., 2011; Wolff et al., 2014). Subsequent deactivation of the BLA via injection of clozapine-N-oxide (CNO), the designer drug, prior to exposure to stressors obliterated the surge of osteocalcin in AAV-injected but not in sham-injected mice (Figures 1J, S1D-E). These data indicate that stressors must signal in the BLA to trigger the release of bioactive osteocalcin, though they do not exclude the possibility that other regions of the brain are also implicated in the development of an ASR.

Bioactive osteocalcin is released from cells of the osteoblast lineage during an acute stress response

The stressor-induced surge in circulating bioactive osteocalcin levels described above occurs independently of sympathetic signaling through β-adrenergic receptors, a well-known regulator of osteoblast functions (Takeda et al., 2002); of circulating adrenal steroid hormones levels; or of transcriptional events in bones or other tissues (Figures 2A-C, S2A-D). This led us to search for other mechanisms that would account for the release of bioactive osteocalcin into general circulation during an ASR.

Osteocalcin is activated through decarboxylation, a reaction that occurs in the bone resorption lacunae (Karsenty and Olson, 2016). However, circulating bioactive osteocalcin (osteocalcin) levels increased equally well in stressor-exposed *oc/oc* mice that lack functional osteoclasts (Scimeca et al., 2000) as in control mice (Figure 2D). They also increased equally well in stressor-exposed WT mice treated with alendronate, an inhibitor of bone resorption (Azuma et al., 1995), or with vehicle (Figures S2E-F). In agreement with these observations, circulating levels of CTX, a biomarker of bone resorption, or of RankL, an activator of bone resorption, did not increase within minutes in stressor-exposed WT mice (Figures S2G-I). In view of these observations we considered the possibility that cells of the osteoblast lineage (osteoblasts and osteocytes) that synthesize osteocalcin are the ones releasing its bioactive form during an ASR. In support of this notion, we found that exposure

to stressors increased circulating bioactive osteocalcin even further in $Tph1_{villin}^{-/-}$ mice, which have twice as many cells of the osteoblast lineage as in control littermates but have normal bone resorption (Figure 2E) (Yadav et al., 2008). In contrast, exposure to stressors did not increase circulating bioactive osteocalcin in $\alpha_1(I)\ Collagen^{DTA}$ mice, which have markedly fewer osteoblasts than WT mice (Figure 2F) (Yoshikawa et al., 2011).

To determine if the release of bioactive osteocalcin is triggered by molecule(s) present in the general circulation and that signal in cells of the osteoblast lineage, we cultured osteoblasts obtained from WT mice in the presence of sera obtained from either unstressed or stressed *Osteocalcin*−/− (*Ocn*−/−) mice. In this experimental setting, the osteocalcin molecules detected in the supernatant can only originate from the cultured osteoblasts. We found that WT osteoblasts produced similar amounts of bioactive osteocalcin whether they were cultured in the presence of sera from unstressed or stressed *Ocn*−/− mice, and none of the specific hormones tested in serum-free conditions increased the release of bioactive osteocalcin by osteoblasts (Figures S2J-K). In contrast, blocking neuronal activity with the peripheral ganglionic blocker chlorisondamine prevented the increase of circulating bioactive osteocalcin in stressor-exposed WT mice, thus suggesting a neuronal mediation of the effect of stressors on circulating bioactive osteocalcin levels (Figure 2G).

Glutamate mediates the stressor-induced release of bioactive osteocalcin from osteoblasts

Among all the neurotransmitters tested, only glutamate (Talman et al., 1980; Toyota et al., 2018) significantly increased the amount of bioactive osteocalcin found in the supernatant of mouse osteoblasts (Figure 3A). In agreement with the data presented in Figure S2J, circulating glutamate does not change in WT mice exposed to stressors (Figure 3B). On the other hand, ablating peripheral glutamatergic neurites using a pegylated diphtheria toxin that does not cross the blood brain barrier (Pereira et al., 2017) (PEG-DT) injected into mice with a conditional diphtheria toxin receptor driven by *Vglut2-Cre* (Vong et al., 2011) ($Vglut2^{iDTR}$ mice), prevented the stressor-induced increase in circulating bioactive osteocalcin (Figures 3C, S3A-C). In addition, we observed that glutamatergic neurites are present in bone and abut osteoblasts (Serre et al., 1999) (Figure 3D). These results suggest that glutamate action on cells of the osteoblast lineage can originate from neurites within bone. These VGLUT2-positive neurites present in bones are tyrosine hydroxylase (TH) negative and do not express any of the markers of sensory neurons tested (Figure 3D and 3E). We note that the existence of a subpopulation of VGLUT2-positive, TH-negative neurons has been previously reported (Brumovsky et al., 2011a; Brumovsky et al., 2011b; Furlan et al., 2016).

A single glutamate transporter, *Eaatl* or *Glast* (Mason et al., 1997; Rothstein et al., 1996), is expressed three orders of magnitude higher in osteoblasts than any other glutamate transporter and than in any other cell type tested, including osteoclasts (Figures 3E, S3F). The role of glutamate transport in osteoblasts through Glast in the release of osteocalcin was delineated in several ways. First, incubation with radiolabeled glutamate significantly increased the intracellular concentration of glutamate in WT but not *Glast*−/− osteoblasts; second, UCPH102, a specific inhibitor of Glast function (Haym et al., 2016), prevented the

uptake of radiolabeled glutamate by WT mouse osteoblasts; third and unlike what is the case in WT osteoblasts, glutamate could not stimulate the release of osteocalcin from UCPH102-treated WT or *Glast*−/− osteoblasts; fourth and in vivo, circulating bioactive osteocalcin did not increase nearly as much in *Glast*−/− as in WT mice exposed to stressors (Figures 3F-I, S3G); and fifth, glutamate prevented the ability of GGCX (Presnell and Stafford, 2002) to carboxylate osteocalcin, whereas aspartate, the closest relative to glutamate that is also transported by Glast, did not (Figure 3J). Accordingly, glutamate could not stimulate the release of bioactive osteocalcin from WT osteoblasts treated with warfarin, a potent inhibitor of GGCX activity (Figure 3G) (Rost et al., 2004). We should emphasize that the inhibition of osteocalcin carboxylation by glutamate was observed at glutamate concentrations similar to or below those that have been reported at glutamatergic synapses (Clements et al., 1992). Taken together these data indicate that the entry via Glast of glutamate into cells of the osteoblast lineage favors the quick release of bioactive osteocalcin by exerting a competitive inhibition of the GCCX during an ASR.

Next we assessed whether signaling in the amygdala affects the release of bioactive osteocalcin, used here as a readout of neuronal signaling in bone. For that purpose, an AAV encoding the stimulatory DREADD hM3Dq was injected into the baso-lateral amygdala (BLA). Subsequent activation of the BLA via injection with clozapine-N-oxide, the designer drug, led to a two-fold increase of circulating bioactive osteocalcin (Figures 3K, S3H).

Osteocalcin signaling in peripheral organs is necessary to mount an ASR

To determine whether the surge of circulating bioactive osteocalcin that is observed in stressor-exposed animals contributes to the development of an ASR, we studied physiological processes that increase within minutes during an ASR and can be reliably monitored in mice. These are: an increase in energy expenditure and circulating glucose, a rise in temperature, a faster heart rate, a more efficient respiration as measured by arterial spO2, an indicator of respiratory oxygenation of arterial blood if there is no change in hemoglobin levels, and Newtonian airway resistance.

Unlike what we observed in WT littermates, *Ocn*−/− mice experienced only a modest increase in energy expenditure, circulating glucose, temperature, heart rate, and respiratory oxygenation of arterial blood upon exposure to stressors (Figures 4A-G, S4A-B). To determine if osteocalcin signals peripherally and/or centrally to enhance these physiological functions during an ASR, we analyzed heart rate and oxygenation of arterial blood in mice lacking Gprc6a, a receptor that only mediates osteocalcin's peripheral functions, and in mice lacking Gpr158, a receptor that mediates osteocalcin signaling in the brain (Khrimian et al., 2017). Both parameters were significantly decreased in *Gprc6a*−/− but not *Gpr158*−/− mice exposed to stressors (Figures 4H-L, S4C-D). Taken together these data indicate that osteocalcin signaling in peripheral organs through Gprc6a is necessary for an ASR to unfold.

Osteocalcin inhibition of the parasympathetic tone triggers an ASR

How does osteocalcin signaling in peripheral organs favor the development of manifestations of an ASR? To address this question we first explored the relationship between osteocalcin and the sympathetic arm of the autonomic nervous system because the

sympathetic tone is a mediator of the ASR and osteocalcin favors catecholamine synthesis in the brain (Karsenty and Olson, 2016). However, we found that circulating norepinephrine, its urinary elimination, its content in the lungs, *Ucp1* expression in brown fat, TH protein content in the heart, accumulation of phospho-CREB (a marker of adrenergic signaling) in the heart and expression of various adrenergic receptors in the trachea and heart were all similar in *Ocn*−/− and WT littermates (Figures S5A-H). Since these markers represent only an indirect measure of the sympathetic tone, we also performed direct electrophysiological recordings of sympathetic nerve activity. This study showed no significant change in renal sympathetic tone after intravenous injection of osteocalcin (Figure 5A). Taken together these data do not provide support for the idea that bioactive osteocalcin would regulate the sympathetic tone in peripheral organs.

This led us to test whether it is by inhibiting the parasympathetic tone that osteocalcin drives an ASR. In support of this notion, we observed that expression of *Choline acetyl transferase* (*Chat*), *Choline transporter1* (*Cht1*) and *Vesicular acetylcholine transporter 1* (*Vacht1*) that are all needed for acetylcholine (ACH) synthesis and recycling (Eiden, 1998) was significantly increased in the trachea and heart of *Ocn*−/− and *Gprc6a*−/− mice, whereas expression of *Chat* in the brain stem was similar in *Ocn*−/− and WT littermates (Figures 5D-E, S5I). Conversely, injections of bioactive osteocalcin decreased expression of these three genes in the trachea and heart of WT mice (Figures S5J-K). More directly, intravenous administration of osteocalcin caused a rapid and significant decrease in the hepatic parasympathetic nerve activity measured in WT mice (Figures 5B, S5L). Thus, bioactive osteocalcin appears to regulate the function of post-ganglionic parasympathetic neurons. The absence of inhibition of the parasympathetic tone in *Ocn*−/− and Gprc6a−/− mice provides an explanation for why heart rate variability and circulating levels of gastrin, whose secretion is promoted by the parasympathetic tone (Perry et al., 2016; Viviani et al., 2011; Vizi, 1973), were significantly higher in *Ocn*−/− and *Gprc6a*−/− mice than in control mice (Figures S5M-P). Finally, exposure to TMT caused a marked decrease in the hepatic parasympathetic nerve activity in WT mice but could not do so in *Ocn*−/− mice (Figure 5C).

To determine where bioactive osteocalcin signals through Gprc6a to allow manifestations of an ASR to develop, and in the absence of a Cre-driver specific to post-ganglionic parasympathetic neurons, we performed multiple experiments.

First, we observed that bioactive osteocalcin directly decreased contraction of WT but not *Gprc6a*−/− tracheal rings within minutes (Figures 5F, S5Q). This effect was dependent on ACH signaling since it was inhibited by atropine, a muscarinic receptor inhibitor (Longo, 1966) (Figure S5R). Of note, the fact that bioactive osteocalcin prevented contraction of human tracheal rings in this assay suggests that osteocalcin inhibits the parasympathetic tone in humans as well (Figure 5G). Second, bilateral cervical vagotomy, a procedure that eliminates parasympathetic signaling to the lungs, corrected the bronchoconstriction and slow heart rate in *Ocn*−/− mice (Figures 5H-I). Third, and in view of the results presented above, we used mice expressing *Green fluorescent protein* (*Gfp*) under the control of *Gprc6a* regulatory elements to determine whether this receptor was expressed in post-ganglionic parasympathetic neurons. This analysis effectively showed that *Gprc6a* is expressed in cholinergic post-ganglionic parasympathetic neurons in the upper airways and the cardiac

ganglia but not elsewhere in these organs (Figures 5J, S5S-T). Fourth, and in the absence of mutant mice lacking Gprc6a only in postganglionic parasympathetic neurons, we generated WT and *Gprc6a*−/− mice that express *Tomato* under the control of the *Chat* promoter to mark parasympathetic neurons (Figure S5U). We then isolated parasympathetic neurons from WT or *Gprc6a*−/− mice and performed patch-clamp electrophysiology studies in the presence or absence of osteocalcin. In the conditions of this assay, bioactive osteocalcin decreased the frequency of action potentials by more than 70% in WT but not in *Gprc6a*−/− tracheal neurons (Figure 5K, 5M). Firing frequency was restored to normal values 10 minutes after washout (Figure 5M). Moreover, sera from stressed *Ocn*−/− mice increased firing of tracheal neurons at least 30-fold more than sera from stressed WT mice (Figure 5L). Taken together these results show that a hormone, osteocalcin, inhibits the activity of post-ganglionic parasympathetic neurons in the context of an ASR, thus leaving the sympathetic tone unabated.

High circulating osteocalcin levels account for the ability of adrenalectomized mice to develop an ASR

Glucocorticoid hormones have been known for decades to potently inhibit *Osteocalcin* expression and production in rodents and humans (Di Somma et al., 2003; Morrison et al., 1989). In full agreement with this notion, adrenalectomized (ADX) WT mice or rats that have undetectable circulating levels of corticosterone have several-fold higher circulating bioactive osteocalcin before and after exposure to stressors than sham-operated ones (Figures 2B, S6A). Hence, we reasoned that ADX mice or rats would be useful tools to determine whether high circulating bioactive osteocalcin levels might be sufficient to allow the development of an ASR in animals lacking both adrenal steroid hormones and adrenal-derived catecholamine.

We found that following exposure to stressors, energy expenditure, temperature, heart rate, and respiration increased equally well in ADX and sham-operated WT mice (Figures 6A-E). Likewise, ADX WT rats that had no circulating corticosterone developed an efficient ASR as determined by a rise in body temperature and heart rate after restraint (Figures 6F-G). Similar observations have been made in adrenal-insufficient dogs that were stressed, and in humans, heart rate, blood pressure and energy expenditure increase to the same extent in glucocorticoid-deficient patients and control individuals who are exposed to a stressor-like high intensity exercise (Mersebach et al., 2003; Zuckerman-Levin et al., 2001). Thus, the ability to develop an ASR in the absence of glucocorticoid hormones is conserved in rodents and humans.

To test the hypothesis of the ability of ADX animals to develop an ASR, we used ADX *Ocn* +/− mice that have normal circulating bioactive osteocalcin levels (Figure 6H). When ADX *Ocn*+/− mice were exposed to stressors, the increase in energy expenditure, heart rate and blood oxygenation that was seen in stressed ADX WT mice was absent or markedly blunted (Figures 6I-L). ADX *Ocn*−/− mice also could not mount an ASR (Figures 6I-L). These results support the notion that, in the mouse, an increase in circulating bioactive osteocalcin levels is sufficient to trigger the development of an ASR.

Further supporting the notion that increasing circulating bioactive osteocalcin levels is sufficient to trigger manifestations of an ASR, we observed that a single injection of exogenous osteocalcin significantly increased heart rate, energy expenditure and oxygen consumption in WT mice (Figures 6M-O).

Discussion

This study shows that bioactive osteocalcin (osteocalcin) is necessary to mount cardinal manifestations of an acute stress response (ASR) through its inhibition of the parasympathetic tone (Figure 6P). Osteocalcin also accounts for why animals lacking glucocorticoid and other molecules produced by the adrenal glands can develop a normal ASR. Although they do not exclude the possibility that other organs may contribute to the development of an ASR, these findings support the hypothesis that a purpose of the endocrine functions of bone is to allow animals living in the wild to escape danger.

Regulation of osteocalcin secretion by stressors

The first feature of a stress hormone, i.e. that its circulating levels should increase within minutes after exposure to stressors, is fulfilled by osteocalcin. The increase in circulating osteocalcin was observed after exposure to all stressors tested and it extends from rodents to humans (Camerino et al., 2017; Patterson-Buckendahl et al., 1995), is specific to osteocalcin among hormones and molecules synthesized in bone, occurs after stressors signal in the amygdala and possibly other areas of the brain, and is independent of glucocorticoid, sympathetic signaling and bone resorption. Rather, the stressor-induced increase in circulating osteocalcin depends on glutamate entry into mouse osteoblasts through the transporter Glast (Mason et al., 1997; Serre et al., 1999; Watkins and Jane, 2006).

It has long been known that osteoblasts have the necessary machinery to take up glutamate, yet the functions of glutamate in osteoblasts had remained elusive (Mason et al., 1997; Serre et al., 1999; Skerry et al., 2001). Our work reveals that one such function is to allow the release of bioactive osteocalcin. For that purpose, glutamate is taken up by *Glast* that is expressed in cells of osteoblast lineage in the mouse. Once inside osteoblasts, glutamate inhibits the activity of GGCX, the enzyme that inactivates osteocalcin by carboxylating glutamate residues. Our data suggest that glutamate entering osteoblasts through Glast originates within bones from neurites that are glutamatergic but do not express any markers of sympathetic or sensory neurons. These neurites bear similarities with VGLUT2-positive, TH-negative, neurons that have been previously reported in sympathetic chain ganglia (Brumovsky et al., 2011a; Brumovsky et al., 2011b; Furlan et al., 2016). We remain cognizant that this preliminary characterization does not exclude the possibility that these neurites may originate from sympathetic or sensory neurons and/or that other cellular origins of glutamate may exist. Lastly, the function of glutamate in osteoblasts described here raises the question of whether glutamate may have in other organs (e.g., the liver) secreting carboxylated proteins.

Inhibition of the parasympathetic tone by osteocalcin during the ASR

The second hallmark of a stress hormone is that it should up-regulate key physiological functions recruited during an ASR. Osteocalcin fulfills this second criterion as well by signaling through Gprc6a in postganglionic parasympathetic neurons to inhibit action potential firing and acetylcholine synthesis and recycling in these neurons. Thus, by decreasing the parasympathetic tone osteocalcin signaling leaves the sympathetic tone unopposed and able to trigger an ASR (Figure 6P). We have so far studied a limited number of manifestations of the ASR, chosen based on their importance during an ASR and on the fact that they can be reliably monitored in mice. It remains to be determined whether osteocalcin regulates other physiological functions, e.g., sweating, that are also up regulated during an ASR. Nevertheless, our results provide an explanation for how the parasympathetic tone is inhibited during the ASR (Porges, 1995).

Of note, energy expenditure, a major ASR-related physiological function enhanced by osteocalcin, is not decreased in *Gprc6a*−/− and *Gpr158*−/− mice and neither receptor is expressed in white or brown adipocytes. This suggests that osteocalcin acts through a third, as of yet unidentified receptor to regulate energy expenditure.

Contribution of osteocalcin to the development of an ASR in the absence of adrenal glands

Unlike what was expected, ADX mice and rats that lack, among other molecules, glucocorticoid hormones and catecholamine, display a normal ASR and similar observations have been made in humans. This feature that underscores the importance of bone as a stress organ, is explained by the existence of high circulating osteocalcin levels in the absence of glucocorticoid hormones, which are well-known repressors of *Osteocalcin* expression (Di Somma et al., 2003; Morrison et al., 1989).

In view of our results, the inhibition of *Osteocalcin* expression by corticosterone raises at least two novel questions. How do circulating osteocalcin levels increase after stress in WT mice? What is/are the physiological purpose(s) of the increase in circulating corticosterone levels during the ASR? We should emphasize that our results do not exclude the possibility that other organs may be implicated in mediating the ASR.

Osteocalcin as a fitness hormone

Osteocalcin enhances multiple physiological processes in peripheral organs and in the brain. At first glance, these functions seem unrelated to each other, an observation that has long raised the question of whether a single rationale could be inferred for the various functions of osteocalcin. The present characterization of osteocalcin as a stress hormone provides a conceptual framework that can capture most osteocalcin-regulated physiological processes. Indeed, the ability of osteocalcin to facilitate the acute stress response, favor memory and enhance muscle function during exercise suggests that osteocalcin confers a survival advantage to bony vertebrates that live in a hostile environment such as the wild. This is particularly relevant in younger rodents and primates that have high circulating osteocalcin levels (Mera et al., 2016). In these younger animals osteocalcin acts as a fitness hormone. An unusual aspect of osteocalcin is that it exerts all of its functions in part in an indirect

manner, i.e., by up-regulating the expression of hormones, cytokines or neurotransmitters. This ability of osteocalcin to increase or decrease the secretion of various regulatory molecules could however be a double-edged sword. For instance, osteocalcin inhibition of the parasympathetic tone could, if occurring at rest, have adverse consequences by constantly maintaining a high sympathetic tone. This may explain why osteocalcin functions seem to take place preferably during stress and/or exercise.

There are obvious similarities between the sympathetic nervous system and osteocalcin signaling. Indeed, both signaling mechanisms are most useful when animals find themselves in life threatening situations and need to rapidly mobilize energy and increase muscle function in order to escape am acute danger. In that regard we note that osteocalcin favors the sympathetic tone either directly in the brain (Oury et al., 2013) or indirectly in peripheral organs (this study). Even though other explanations can be proposed, we hypothesize that the same fitness and survival purpose animates the structural and ambulatory functions of bone in the wild as well.

Osteocalcin as an anti-geronic molecule

Osteocalcin is not only necessary to up-regulate the aforementioned physiological functions, it is also sufficient to do so to the extent that it can reverse manifestations of aging in the brain and in muscle. This ability of exogenous osteocalcin to reverse in the mouse, objective manifestations of aging such as memory loss and decreased muscle function, together with the fact that its circulating levels plummet with age when memory, muscle function and fertility all decrease, suggest that osteocalcin is also an antigeronic hormone (Mera et al., 2016; Khrimian et al., 2017). Going forward, these observations are an impetus to determine whether the biology of osteocalcin could be harnessed to treat deleterious manifestations of aging such as age-related memory loss and a decrease in muscle function, among others, in humans.

Limitations of the study

While our study shows that osteocalcin is released from bone during an ASR in a glutamate dependent manner and that once released it mediates several cardinal manifestations of the ASR, there still are questions that remain to be addressed. For instance, our experiments have not determined the origin or molecular identity of glutamatergic neurites within bone nor have they defined the intracellular signaling pathway whereby osteocalcin inhibits parasympathetic activity.

STAR Methods

LEAD CONTACT AND MATERIALS AVAILABILITY

Further information and requests for reagents and/or data can be directed to the Lead Contact, Gerard Karsenty (gk2172@cumc.columbia.edu). Any sharing of materials or data may be subject to material transfer agreements and/or data-sharing agreements per the requirements of the study sponsors. Otherwise, any reagents used in this study can be made available upon request.

EXPERIMENTAL MODEL AND SUBJECT DETAILS

Animal Models—All animals of the same batch were born within an interval of 2 weeks and were kept in mixed genotype groups of 2-5 females in the same cage, at standard laboratory conditions (12 hr light/dark cycle, 22-25 °C, PicoL ab Rodent Diet 5053 and water ad libitum). For all experiments, we randomized mice into experimental groups and used females and littermates as controls unless otherwise stated. *Ocn*−/− (*osc*^{m1}/*osc*^{m1}) were previously described (Ducy et al., 1996), in brief, null alleles replace both the *Bglapl* and *Bglap2* genes. *Gpr158*−/− (Gpr158$^{tm1.1(KOMP)Vlcg}$) mice were purchased from the KOMP repository (VG10108). This mouse line was made by the insertion of a LacZ cassette with a stop codon in the first two exons of *Gpr158* (Orlandi et al., 2015). *Gprc6a*−/− mice were described previously (Oury et al., 2011). *Oc/oc* mice, maintained on a C57BL/6J background, were obtained from Dr. Anne Villa and, in brief, contain a spontaneously occurring null mutation in *Tcirg1*. *Tph1*$_{vil}$*fl/fl* maintained on a C57BL/6J background were described previously (Yadav et al., 2008) and in brief are homozygous for floxed *Tph1* alleles which are null when recombined as well as one allele of *Vil-cre*. *Vglut2-cre* mice maintained on a C57BL/6J background were obtained from Jackson Laboratory and were described previously (Vong et al., 2011) and in brief contain Cre knocked-in to the *Vglut2* locus. iDTR mice, maintained on a C57BL/6J background, expressing a floxed stop cassette driving DTR in the Rosa26 locus, were obtained from Jackson Laboratories and were described previously (Cichon and Gan, 2015). To generate the *Gprc6a-gfp* mouse line, maintained on a C57BL/6J background, *P2A-EGFP-PolyA* was inserted into the *Gprc6a* gene locus of BAC RP23 before the *Gprc6a* TGA stop codon using previously described recombineering methods (Xing et al., 2013). The BAC transgene was then injected into pronuclei from B6CBAF2 mice. Mice were genotyped using primers: GFP forward 5'-GGTGAACCGCATCGAGC and GFP reverse 5'- GTCAGCAAACACAGTGCACA. To generate the *Glast*−/− mouse line, maintained on a C57BL/6J background, guide RNA sequences were selected flanking Exon 4 of the *Glast* gene using the MIT CRISPR Design Server. Two Guide RNAs flanking exon 4, TracrRNA (IDT) and Cas9 protein (IDT) were injected into C57BL/6N eggs to generate *Glast* null progeny. Deletion of exon 4 of the *Glast* gene was confirmed by sequencing and PCR genotyping. DTA mice were obtained from Dr. S. Kousteni (Yoshikawa et al., 2011) and in brief contain an *Cre* inducible DTA cassette. WT 129S6/SvEvTac mice were purchased from Taconic Biosciences and C57BL/6J from Jackson Laboratory. Upon arrival at the animal facility, mice were housed at least 2 weeks before performing experiments. *Gpr158*−/− mice were maintained on a 129-Sv/C57BL/6J mixed genetic background. *Gprc6a*−/− mice were maintained on a 129-Sv/C57BL/6J mixed genetic background. *Ocn*−/− mice were maintained on a 129-Sv background. Mice were housed five animals per cage (polycarbonate cages (35.5 × 18 × 12.5 cm)), under a 12 h light/dark cycle with ad libitum access to standard mouse chow and water prior to experimentation. All PCR oligonucleotides used for genotyping of any of the mice are available upon request. All experiments involving animals were approved by the Institutional Animal Care and Use Committee of Columbia University Medical Center.

Human sample osteocalcin measurements—The acute stress was carried out as previously described (Prather et al., 2009) under University of Pittsburgh IRFB -- #0307004. Consent was obtained and subjects of both sexes were aged between 41-58 years and were

in good health with no record of serious illness sample size was determined based on previously performed studies (Prather et al., 2009). In short, subjects engaged in a 10-minute evaluative speech task and blood was sampled before, immediately after and 30 minutes after the completion of the test. Circulating levels of bioactive osteocalcin in humans was estimated using a bioactive osteocalcin ratio according to a recently published method (Bonneau et al., 2017) that has greatly improved the accuracy of detecting undercarboxylated osteocalcin levels in human serum to within a 4.5-5.7% coefficient of variability. For human samples, separate ELISAs are used to measure total osteocalcin levels (ALPCO, 38-OSTHU-E01) and carboxylated osteocalcin levels (Takara Bio, MK111). Briefly, total and fully carboxylated osteocalcin levels were normalized to pre-stress levels and then undercarboxylated osteocalcin level was estimated for each participant by dividing Gla17-OCN by total-OCN.

Cell Culture—Mouse calvaria osteoblasts were isolated and cultured as described previously (Ferron et al., 2010). In brief, calvaria of 2-5 day old mice of both sexes were dissected and digested in collagenase Type 2 (Worthington) and differentiated for 7-10 days in Alpha-MEM (Gibco), 5 mM beta-glycerophosphate (Sigma) and 100 ug/ml ascorbic acid (Sigma) at 37 °C 5% CO_2.

METHODS DETAILS

Stress—All animals of the same batch were born within an interval of 2 weeks and were kept in mixed genotype groups of 2-5 females in the same cage, at standard laboratory conditions (12 hr light/dark cycle, constant room temperature and humidity, and standard lab chow and water ad libitum). For each test, mice were transported a short distance from the holding mouse facility to the testing room in their home cages. Mouse weight was between 22g and 32g. Unless otherwise indicated, baseline blood was taken 48 hours prior to onset of stress. In the case of the time course experiment, each time point represents a separate batch of mice exposed to the indicated time period of stress. Stress was delivered by an experimentalist blind to the genotypes or treatment of the mice under study. For 2,3,5-Trimethyl-3-thiazoline (TMT) stress, food and water were removed immediately prior to TMT exposure. A cotton swab containing 10uL of TMT (Scotts Canada Ltd. 300000368) was placed in the home cage for 15 minutes. Serum was collected after 15 minutes of TMT exposure, and mice were transferred to a fresh home cage free of TMT odor. Exposure to rabbit urine (Kishel Scents, USA) was performed using the same procedure as that used for exposure to TMT. For foot shock stress, mice were placed in a conditioning apparatus (Med Associates, USA), which had a floor of stainless steel bars wired to a shock generator. They received 3 foot shocks (1 sec, 1 mA), which were administered at time points of 60, 120 and 180 seconds after the animals were placed in the chamber. Blood was collected 15 minutes after onset of stress. For restraint stress, mice were placed in modified 50 mL Falcon tubes with holes allowing normal breathing. Blood was collected 45 minutes after onset of restraint stress. For rat experiments, 12-week-old female Sprague-dawley rats were exposed to restraint stress for 30 minutes.

***In Vivo* Treatments—**Mice were injected with nadalol intraperitoneally (i.p.) with either vehicle or 72 mg/kg of nadolol (Sigma, N1892) 30 minutes prior to onset of acute stress. Blood was taken from the submandibular vein of all mice 15 minutes after onset of stress.

Mice were injected i.p. with either vehicle or 72 mg/kg of Alendronate sodium (Sigma, 1012780) every other day for 14 days prior to onset of acute stress. Blood was taken from the submandibular vein of all mice 15 minutes after onset of stress. TMT stress was performed as described above. Vertebrae were then harvested for bone histomorphometric analysis.

Mice were injected i.p. with either vehicle or .07 mg/g tamoxifen (Sigma, T5648) every day for 10 days. All experiments were performed between day 10 and day 20. TMT stress was performed as described above. Four hours after treatment, mice were sacrificed and organs were collected for gene expression.

Control or $Vglut^{DTR}$ Mice were injected i.p. with either vehicle or 8.3 ng/g PEG-DT (Ana Domingos) every day for 5 days. All experiments were performed between day 5 and day 8. TMT stress was performed as described above. 24 hours after final treatment, mice were sacrificed and organs were collected for histology.

Mice were injected i.p. with either vehicle or 32 mg/kg of chlorisondamine (Sigma, C5366) 30 minutes prior to onset of acute stress. Blood was taken from the submandibular vein of all mice 15 minutes after onset of stress. TMT stress was performed as described above.

For measurement of *Chat*, *Cht1* and *Vchtl* expression in trachea and heart, WT mice were injected i.p. with either 30 ng/g or 100 ng/g of recombinant osteocalcin and returned to their home cage. Four hours after treatment, mice were sacrificed and organs were collected for gene expression.

For the measurement of heat, VO2 and heart rate after osteocalcin injection, WT mice were injected i.p. with 10 ng/g of recombinant osteocalcin and heart rate was monitored for 5 minutes using the MouseOx (Starr Life Sciences) protocol described below.

For measurement of circulating osteocalcin, WT mice were injected i.p. with .25 mg/kg of D,L-(Tetrazol-5-yl)glycine (TZG) and returned to their home cage. One hour after treatment, blood was collected from submandibular vessel. One mouse experienced a seizure and this mouse was excluded from the study.

Bone Histomorphometry—Bone histomorphometry analyses were performed on L3 and L4 vertebrae as described previously (Wei et al., 2015), in brief vertebrae were embedded in methyl methacrylate and sectioned. Von Kossa, Van Gieson, and toluidine blue staining were performed to measure mineralized bone volume over the total tissue volume (BV/TV) and osteoblast number per tissue area (N.Ob/T.Ar).

Adrenalectomy—In mice and rats a mid-dorsal skin incision was made at the level of the first through third lumbar vertebrae. The incision was moved laterally to expose the paracostal musculature. An incision was made just caudal to the 13th rib bilaterally. The

adrenal gland on the left side was visualized by lateral retraction of the spleen. The adrenal gland on the right side was visualized by cranial retraction of the liver. The adrenal gland and its associated fat pad were identified cranial and medial to the kidney and the vessels supplying the gland were crushed with two pairs of hemostats. Using blunt forceps, the entire fat pad was drawn out of the incision and the adrenal gland was removed intact. The muscle was sutured with absorbable suture bilaterally. The skin incisions were closed with wound clips. After surgery animals were provided with .9% saline for drinking water to supplement for loss of aldosterone. All experiments were performed after 10 days of post-operative rest.

Energy Expenditure, Heart Rate, Heart Rate Variability, Lung Function, Temperature and Glucose Measurements—Mice were acclimated for at least 12 hours prior to recording in energy expenditure cages (Oxymax-CLAMS, Columbus Instruments). From 12pm to 7pm the following day, the normal cage bottom was replaced with a modified shock grid floor and baseline readings were taken until 6pm. At 6 pm, five 1-second, 1mA shocks were applied over 2.5 minutes. Data is represented as pre-shock and 1h post-shock.

To measure heart rate and arterial oxygen saturation in mice, five days prior to experimentation a plastic sham collar (Starr Life Sciences) was placed on the mouse for 5 minutes for acclimation. On the day of the experiment, the MouseOx Collar Sensor (Starr Life Sciences) was placed on a mouse that was then acclimated for 30 minutes in the conditioning apparatus (Med Associates, USA). After 15 minutes, 5 minutes of baseline parameters were recorded followed by five 1-second, 1mA shocks applied one per minute over 5 minutes. Heart rate and SpO2 at baseline and 5 minutes after the onset of stress are reported. To measure Newtonian airway resistance, blood pressure and heart rate in mice, measurements of pulmonary mechanics were done as previously described (Arteaga-Solis et al., 2013) using the forced oscillation technique with a flexiVent (SCIREQ, CA). The mice were sedated with an i.p. injection of pentobarbital (50 mg/kg). A tracheostomy was performed with an 18 G cannula, and the mouse was connected to the flexiVent. EKG leads were placed on the extremities, and the right carotid artery was cannulated and connected to the blood pressure transducer connected to the flexiVent. The mice were ventilated at 150 Hz, tidal volume (VT) 10 ml/kg, and positive end-expiratory pressure (PEEP) level of 3 cmH2O. To ensure identical volume history profiles, the lungs were first inflated to three times the VT and ventilated for 10 minutes. For vagotomy, mice were ventilated on the flexiVent and after 5 minutes of baseline recordings bilateral cervical vagotomy was performed. Heart rate variability is measured as the square root of the variance between NN intervals. For measurement of temperature, mice and rats were kept in their home cage and rectal temperature (Model BAT-12 Physitemp) was taken at −30 and −15 minutes. At 0 minutes mice were given foot shock stress as described above, then rectal temperature was measured again at 15 minutes post stress. For rats, rectal temperature was taken at 0 minutes then again at 15 and 30 minutes after initiation of restraint stress.

For measurement of blood glucose levels, mice were fasted for 4 hours and transported to the testing room at least one hour prior to the start of experimentation. Circulating glucose was measured using an Accu-Chek active blood glucose meter and corresponding test strips

(Roche) on a drop of tail vein blood. Time 0 was collected immediately before foot shock stress.

Immunohistochemistry and Histology—Immunofluorescence of lumbar spinal chord, femur, airway ganglia (trachea), cardiac ganglia, white adipose tissue and brain was performed on 16mm slices of frozen tissue fixed with 4% PFA in 0.1M sodium phosphate buffer, pH 7.4. Sections were permeabilized and blocked with 0.5% Triton in Tris buffered saline, pH 7.4 and 5% normal donkey serum. After blocking, sections were incubated with primary antibodies overnight at 4°C. For femur tissue, samples were de calcified for 24 hours in 0.5 M EDTA pH 7.4 according to previously described protocols (Kusumbe et al., 2015). The following antibodies were used for this assay: anti-VGLUT2 (1:300) (Synaptic Systems, 135403), anti-VGLUT2 (1:300) (Abcam, ab29157), anti-III Tubulin (1:500) (Abcam, 2G10), anti-GFP (1:300) (Abcam, ab13970), anti-Vacht1 (1:200) (Millipore, ABN100), anti-MCherry (1:300) (Abcam, ab167453), anti-OCN C-Terminal (1:300) (Karsenty lab), anti-TH (1:300) (Millipore, ab1542), anti-NF200 (1:300) (Millipore, ab5539), IB4 isolectin (Thermo Fisher Scientific, I23450), anti-PVALB (Swant, PVG-213), anti-PGP9.5 (Millipore, ab5925), and anti-CGRP (Sigma, C8198). Sections were washed three times in Tris buffered saline, pH 7.4, followed by an incubation with secondary antibodies (Invitrogen, 1:200) diluted in blocking solution and were incubated 1h at RT. After three washes with Tris buffered saline, pH 7.4, sections were mounted with DAPI Fluoro-Gel (Electron Microscopy Sciences) and visualized using a Nikon Ti Eclipse microscope. When multiple experimental groups were present slides were blinded. Images were analyzed using ImageJ v2.0. Airway ganglia (trachea) of *Chat-tdTomato* mice were not fixed and instead mounted directly on a slide with Flouro-Gel and imaged and analyzed as described above.

Gene Expression Analysis by qPCR—All dissections were performed under a Leica MZ8 dissecting light microscope. Adrenal weights were measured using a Mettler Toledo New Classic MS analytical scale. All organs were snap frozen in liquid nitrogen and kept at −80 °C until use. Total RNA was isolated using TRIzol (Invitrogen). Total RNA was first incubated with DNAse I for 30 minutes at room temperature to remove any genomic DNA. DNAse I-treated total RNA was converted to cDNA by using M-MLV reverse transcriptase (Thermo, 28025013) and random hexamers (Thermo, N8080127). qPCR was performed on a CFX96 Touch™ Real-Time PCR Detection System (Bio-Rad) and analyses were done using specific quantitative PCR primers and expressed relative to *Hprt* levels.

Recombinant Osteocalcin—Mouse uncarboxylated osteocalcin was purified from BL21 transformed with pGEX2TK-mOCN as described (Lee et al., 2007; Mera et al., 2016). Briefly, GST-osteocalcin fusion protein was produced in BL21 pLyS transformed with pGEX2TK-mOCN after induction with IPTG. Cells were collected in lysis buffer (PBS 1X, 10mM Tris pH 7.2, 2mM EDTA, 1% Triton and 1X protease and phosphatase inhibitor cocktail (Thermo, 78443). Following 4 freeze/thaw cycles and sonication, lysates were cleared by centrifugation. The supernatant was incubated with glutathione-sepharose 4B (GE, 17075601) for 4 hours at 4 °C. Following 6 washes with washing buffer (PBS 1X, 1% Triton) and with PBS 1X, osteocalcin was then cleaved out from the GST moiety by using

thrombin (GE, 27-0846-01). Four fractions were collected and each of them was incubated with Benzamidine sepharose (GE, 17-5123-10) for 30 minutes at room temperature to remove thrombin.

Immunoblotting—Frozen tissue were pulverized in lysis buffer (20 mM Tris-HCl (pH 7.65), 150 mM NaCl, 1 mM EDTA, 1 mM EGTA, 1% Triton) supplemented with 1X protease and phosphatase inhibitor cocktail (Thermo, 78443). Lysates were clarified by centrifugation and protein concentration was determined by a Bradford assay. Clarified samples were heated at 65 °C in Laemmli buffer for 5 minutes. Proteins were run on an SDS-PAGE gel and transferred to nitrocellulose membrane (Bio-Rad, 1620112). Membranes were blocked with TBST-5% BSA for 1 hour, incubated with primary antibody overnight at 4 °C and probed with HRP-conjugated antibodies for 1 hour at room temperature. The following antibodies were used in this study: anti-a-tubulin (1:5000, Sigma, T6199); anti-RankL (1:5000, Abcam, ab45039) and anti-Type-I-collagen (1:5000, Rockland Immunochemicals, 600-401-103-0.5), anti-TH (Cell Signaling, 2792), anti-Phospho- CREB (Cell Signaling, 9198), anti-CREB (Cell Signaling Technology, 9104). Band intensities were quantified using ImageJ software. Dashed lines separating two bands indicate that these bands are on the same membrane but are not adjacent.

Radiolabeled Glutamate Uptake—Glutamate uptake was measured in osteoblasts after 10 days of culture. Cells were washed five times with basal buffer (135 mM NaCL, 3.8 mM KCl, 1.2 mM $MgSO_4$, 1.3 mM $CaCl_2$, 1.2 mM KH_2PO_4, 10 mM glucose, 10 mM HEPES) and then incubated with 1 μM ^3H glutamate (PerkinElmer, NET490001MC), lysed and measured on a scintillation counter. μM of glutamate estimated from CPU count based on standard curve of pure μM of serially diluted ^3H glutamate.

Measurement of Circulating Factors—For either mice or rats, blood was collected from the facial vein into Capiject (Terumo, TM) tubes followed by centrifugation at 15 × *g* for 10 minutes. All serum aliquots were stored at −80 °C until use. Circulating levels of osteocalcin in mouse or rat serum were determined with a specific ELISA previously described (Ferron et al., 2010a; Ferron et al., 2010b). Total levels of osteocalcin and carboxylated osteocalcin were estimated using two different specific antibodies. Bioactive osteocalcin was determined by subtracting the carboxylated osteocalcin levels from total osteocalcin levels (Ferron et al., 2010a; Ferron et al., 2010b). Rate of osteocalcin release was determined by calculating the difference in serum bioactive osteocalcin and dividing by the time elapsed since the onset of stress. CTX (IDS, AC-06F1), PiNP (IDS, AC-33F1), gastrin (Sigma, RAB0200), glutamate (Abcam, ab83389), sclerostin (R&D, MSST00), epinephrine (Abnova, KA1882), norepinephrine (Abnova, KA1891) and Fgf23 (Kainos, CY-4000) were measured according to manufacturer's instructions. NE detection in organs was performed by HPLC as previously described (Arteaga-Solis et al., 2013). Hemoglobin was measured using Element POC (EPOC) rapid blood analyzer (Heska) according to manufacturer's instructions.

In Vitro Procedures—For treatment of osteoblasts, on day 10 of culture, cells were incubated in serum-free media without glutamate for four hours before addition of treatment.

In cells that received warfarin pre-treatment,10 μM of warfarin (Santa Cruz, 129066) was added to the media on days 8 and 9 of culture, then glutamate treatment was performed on day 10. In all groups, supernatant was collected without disturbing cells an hour after onset of treatments on day 10. Treatments included pituitary extract (Thermo Fisher Scientific, 13028014), growth hormone (BioVision, 4770), ACTH (Phoenix Pharmaceuticals, 001-21), TSH (Sigma, T8193), LH (Sigma, L5269), FSH (Sigma, F2293), prolactin (Sigma, SRP4688), MSH (Sigma, M4135), PTH (Sigma, P3921), leptin (Sigma, L3772), insulin (Sigma, I3536), glucagon (Sigma, G2044), dexamethasone (Sigma, D4902), isoproterenol (Sigma, 1351005), orexin A (Phoenix Pharmaceuticals, 003-30), NPY (Bachem, H-6375), dopamine (Sigma, H8502), substance P (Sigma, S6883), CGRP (Phoenix Pharmaceuticals, 15-09), BDNF (PeproTech, 450-02), glutamate (Sigma, 49621) and UCPH-102 (Abcam, 146404). The gamma-carboxylase (GGCX) enzymatic activity assay was performed on recombinant OCN as previously described (Tie et al., 2004).

Tracheal Ring Electrophysiology—Organ bath experiments were performed as previously described (Arteaga-Solis et al., 2013). In brief, 10-week-old male mice tracheal rings were excised and immersed in Kreb-Henseleit (KH) buffer (in mM: 115 NaCl, 2.5 KCl, 1.19 CaCl2, 2.46 MgSO4, 1.38 NaH2PO4, and 5.6 glucose, pH 7.4). The tracheal rings were suspended at 0.5 g resting tension in oxygenated KH buffer at 37 °C on a tissue bath system. The rings were at 0.5 g isotonic force with the following electrical field stimulation: Train: 0.013 Trains/s, Train duration: 5 s, Pulse duration: 0.5 ms, Volts: 24 V, Stimulation rate: 20 Hz. Electrical stimulation was applied using Acqknowledge software from BIOPAC Systems. Trachea rings were treated with either 10^{-6} M atropine (Sigma, A0132) or 10 ng/ml recombinant osteocalcin. Values reported are post-treatment magnitude (in force) of electric field-stimulated contraction normalized by pretreatment contractions.

Electrophysiology—The preparation of trachea parasympathetic postganglionic neurons was performed as described with modifications (Weigand et al., 2015). Briefly, mice on C57B6 genetic background (male and female, 3-4 weeks old) were anesthetized with isoflurane and then sacrificed with cervical dislocation. Then intrathoracic trachea and mainstem bronchi with the vagus nerves attached were removed and dissected in ACSF (bubbled with 95% O_2/5% CO_2) containing (in mM): NaCl 124, KCl 3, $CaCl_2$ 2, $MgCl_2$ 2, NaH_2PO_4 1.23, $NaHCO_3$ 26, glucose 10, pH 7.4 with NaOH. The airways were cut ventrally along the midline, opened as a sheet, and pinned, lumen-side down, to a Sylgard-lined Petri dish. After excess connective tissue and fat were cleared, the trachea was treated with a combination of collagenase (2mg/ml) and dispase (1mg/ml) prepared with modified ACSF without Mg^{2+} and Ca^{2+} for 30 minutes at 37 °C. The tracheal tissue was then transferred to a recording chamber and constantly perfused with bath solution (33 °C) at 2 ml/min for electrophysiological recording. Extracellular recordings were made from identified trachea parasympathetic postganglionic neurons with a glass electrode filled with ACSF (resistance=2-5 MΩ) with a multiclamp 700A amplifier (Molecular Devices). A loose seal was formed (resistance= 10-20 MΩ) when the micropipette touched the surface of a neuron. For experiments involving treatment with sera, WT and *Ocn*−/− mice were exposed to TMT for 15 minutes and blood was collected as described above. Sera from each experimental

group were pooled and aliquoted. After 5-10 minutes of baseline response was recorded, drugs were applied to the recording chamber through bath application.

In Vivo Neural Recordings of Sympathetic and Parasympathetic Nerve Activity —Each mouse was anesthetized with intraperitoneal administration of ketamine (91 mg/kg body weight) and xylazine (9.1 mg/kg body weight). Tracheotomy was performed by using PE-50 tubing to provide an unimpeded airway for the mouse to spontaneously breathe O_2-enriched room air. Next, a micro-renathane tubing (Braintree Scientific, MRE-40) was inserted into the right jugular vein for infusion of the sustaining anesthetic agent (α-chloralose: initial dose of 12 mg/kg, then sustaining dose of 6 mg/kg/h). A second MRE-40 catheter was inserted into the left common carotid artery attached to a pressure transducer (iWorx Systems, Inc., BP-100) for continuous measurement of arterial pressure and heart rate. Core body temperature was monitored through a rectal probe and maintained at 37.5 °C throughout the experiment. Next each mouse was instrumented for sympathetic or parasympathetic nerve recording.

To gain access to the nerve fascicle that innervates the left kidney, a peroneal incision was performed along the left flank between the ilium crest and thoracic ribs. The renal nerve was isolated and placed on a bipolar platinum-iridium electrode (A-M Systems, 36-gauge) and secured with silicone gel (WPI, Kwik-Sil). The electrode was attached to a high-impedance probe (Grass Instruments, HIP-511) and the nerve signal was filtered at a 100- and 1000-Hz cutoff with a Grass P5 AC pre-amplifier and amplified 10^5 times. The nerve signal was then routed to a speaker system and to an oscilloscope (Hewlett-Packard, model 54501A) to monitor the audio and visual quality of the nerve recording. The nerve signal was also directed to a resetting voltage integrator (University of Iowa Bioengineering, model B600c) and finally to a MacLab analog-digital converter (ADInstruments, Castle Hill, New South Wales, Australia, Model 8S) containing software (MacLab Chart Pro; Version 7.0) that utilizes a cursor to analyze the total activity (integrated voltage) and to count the number of spikes/second that exceed the background noise threshold. Under stable plane of anesthesia and strict isothermal conditions (37.5 °C), continuous recording of baseline sympathetic activity was measured over a 10-minute control period. Vehicle or osteocalcin was then slowly administered, and the sympathetic response recorded continuously for the next 120 minutes. To test the responsiveness of the preparation, an intravenous infusion of sodium nitroprusside (20 μg) was administered. The reflex change in sympathetic nerve activity was tabulated at the exact time that peak decrease in arterial pressure occurred.

To access the hepatic parasympathetic vagal nerve the mouse was placed in a dorsal position. An incision was made in the abdominal region below the rib cage to access a chain of the hepatic parasympathetic nerve located on the right lateral side of the esophagus. The hepatic vagal nerve fascicle was carefully isolated from its surrounding connective tissues and attached to a bipolar platinum-iridium electrode. The nerve signal was filtered, amplified and quantified as above. Under stable plane of anesthesia and isothermal conditions (37.5 °C), a continuous recording of basal hepatic vagal nerve activity was measured over a 10-minute control period before vehicle or osteocalcin was slowly administered. The response of hepatic vagal nerve activity recorded continuously for the next 120 minutes.

A separate cohort of *Ocn*−/− and wild type control and female mice were prepared as above for direct hepatic vagal nerve activity recording without the tracheotomy. These mice were able to spontaneously breathe O_2-enriched room air unimpeded through their own nasal passages. With a stable plane of anesthesia and under strict isothermal conditions (37.5 °C), continuous recording of basal hepatic vagal nerve activity was measured for a 30-minute control period. A small cotton swab soaked with 2,5-dihyro- 2,4,5-trimethylthiazoline (TMT) was then placed at the end of the mouse's nose. The effects of TMT on hepatic vagal nerve activity was recorded for the next 60 minutes. The TMT-soaked cotton swab was removed, and the study extended for an additional 30 minutes for a recovery period.

At the conclusion of each study, mice were sacrificed using an overdose of ketamine/xylazine, the hepatic or renal nerve fiber was severed, and the residual background noise was used to normalize the basal nerve activity. Separate mice were used for each nerve recording.

Stereotaxic Injection—Stereotaxic surgery was performed in 3-month-old C57BL/6J male mice obtained from the Jackson Laboratory. Mice were anesthetized with i.p. injection of a mixture of ketamine hydrochloride (100mg/kg of BW - 1000 Virbac) and 100 mg/ml BW xylazine (10mg/kg of BW - Rompun 2%; Bayer) and placed in a stereotaxic frame (900SL-KOPF). Ophthalmic eye ointment was applied to the cornea to prevent desiccation during surgery. The fur in the area surrounding the incision was trimmed and Vetedine solution (Vetoquinol) was applied. 1 μL of 1.4×10^9 vg/μL AAV8.2-hEF1α-hM4Di-mCherry-WPRE (MIT Viral gene Transfer Core) was injected at 100 nL per minute. 1 μL of 2.0×10^9 vg/μL AAV8-hSyn-hM3Dq-mCherry-WPRE (Addgene) was injected at 100 nL per minute. The viruses were injected bilaterally into the basolateral amygdala ((from bregma) AP = −.82 mm, DV = +/−2.80 mm and ML = −5.00 mm) using a 1 μL Hamilton syringe (65458-01). To limit reflux along the injection track, the needle was maintained in place for 10 minute before and after each 1 μL injection. Then, the skin was closed using silk suture and the mice were injected locally with surgical analgesic. Three weeks after injections baseline blood was taken. Two days later mice were injected with 5.0 mg/kg clozapine-N-oxide (CNO) (Sigma, C0832). In the case of hM4Di-expressing mice, CNO was injected one hour prior to acute TMT stress. Then blood was taken 15 minutes after onset of TMT. In the case of hM3Dq-expressing mice, CNO was injected 20 minutes prior to blood collection. Expression of hM4Di-mCherry or hM4Dq-mCherry in the BLA was confirmed in every mouse by post-hoc immunofluorescent histological analysis.

Isolation of Total RNA and Northern Blot Analysis—Total RNA was isolated from different tissues by the TRIzol method. Briefly, mice were exposed to no shock (−) or foot shock (+) and 1 hour later tissues were collected and processed for RNA isolation by TRIzol method according to manufacturer's instructions (Sigma). Seven micrograms of total RNA from each sample were then electrophoresed in a 1% agarose gel containing MOPS (0.02M), sodium acetate (0.005M), EDTA (0.001M), and 5.4% formaldehyde. The RNA was then transferred to Hybond N+ membrane (Amersham Biosciences) in 10× SSC (1.5M sodium chloride and 0.15M sodium citrate) using capillary blotting overnight. The blot was cross-linked and prehybridized at 60 °C in hybridization buffer (0.33M sodium phosphate and

6.66% SDS). The blot was then hybridized at 60 °C for 12 hours with Ocn cDNA probe radiolabelled by random primer labeling with alpha32PdCTP (6,000 Ci/mmol). The blot was washed (2 times, 45 minutes each) at 60 °C in 0.2X SSC with 0.1% SDS and autoradiographed with Kodak Biomax MR film at −80 °C with an intensifying screen for varying duration.

QUANTIFICATION AND STATISTICAL ANALASIS

Data Analysis—All values are depicted as mean ± SEM. Statistical parameters including the exact value of n, post hoc test and statistical significance are reported in every figure and figure legend. Numbers of mice were estimated to be sufficient based on pilot experiment and previously published work (Lee et al., 2007; Mera et al., 2016; Oury et al., 2011). Outlier tests or tests for normality were not performed. Data are estimated to be statistically significant when p≤0.05 by Student's t-test One-way ANOVA or Two-way ANOVA. In every figure an asterisk denotes statistical significance (*p ≤ 0.05; **, p≤ 0.01). Data were analyzed using Graph Pad Prism 7.

Supplementary Material

Refer to Web version on PubMed Central for supplementary material.

Acknowledgements

We thank Drs. Axel, Picard, Emala, Hen, Villa and Rifkin for advice, reagents and reading of the manuscript, T.D. Berger, L. Schultz, Y. Chen, C. Meghir and L. Shi for experimental help, Dr. Neve (MIT Viral Gene Transfer Core) for providing AAV containing the *hM4Di* DREADD construct, Chyuan-sheng Li (Transgenic Mouse shared resource) for help with mouse model design and production. Images were collected in the Confocal Microscopy Shared Resource of HICCC, supported by P30 CA013696 (NCI). This work was supported by 2P01AG032959-06A1 (NIA) (G.K.), 1R01DK104727-03 (NIDDK) (GK), 1R01AR073180-01A1 (NIAMS) (GK), DA040782-01A1 (NIDA) (X.G.), Ramalingaswamy Fellowship (BT/HRD/35/02/2006) Dept. of Biotechnology, India (V.K.Y), CIHR Fellowship 201511MFE-359182-181537 (S.C.), NIDDK Training Grant 5T32DK007328 (J.M.B, L.K.), NIAID Training Grant 5T32DK007328-38 (J.M.B) and the Columbia Aging Center (G.K.) and 2P01HL084207 (NHLBI) (K.R), BX004249 (VA) (K.R) and the Fraternal Order of Eagles Diabetes Research Center (University of Iowa) (K.R.).

References

Arteaga-Solis E, Zee T, Emala CW, Vinson C, Wess J, and Karsenty G (2013). Inhibition of leptin regulation of parasympathetic signaling as a cause of extreme body weight-associated asthma. Cell Metab 17, 35–48. [PubMed: 23312282]

Axelrod J, and Reisine TD (1984). Stress hormones: their interaction and regulation. Science 224, 452–459. [PubMed: 6143403]

Azuma Y, Sato H, Oue Y, Okabe K, Ohta T, Tsuchimoto M, and Kiyoki M (1995). Alendronate distributed on bone surfaces inhibits osteoclastic bone resorption in vitro and in experimental hypercalcemia models. Bone 16, 235–245. [PubMed: 7756053]

Brumovsky PR, Robinson DR, La JH, Seroogy KB, Lundgren KH, Albers KM, Kiyatkin ME, Seal RP, Edwards RH, Watanabe M, et al. (2011a). Expression of vesicular glutamate transporters type 1 and 2 in sensory and autonomic neurons innervating the mouse colorectum. J Comp Neurol 519, 3346–3366. [PubMed: 21800314]

Brumovsky PR, Seroogy KB, Lundgren KH, Watanabe M, Hokfelt T, and Gebhart GF (2011b). Some lumbar sympathetic neurons develop a glutamatergic phenotype after peripheral axotomy with a note on VGLUT(2)-positive perineuronal baskets. Exp Neurol 230, 258–272. [PubMed: 21596036]

Camerino C, Conte E, Caloiero R, Fonzino A, Carratu M, Lograno MD, and Tricarico D (2017). Evaluation of Short and Long Term Cold Stress Challenge of Nerve Grow Factor, Brain-Derived Neurotrophic Factor, Osteocalcin and Oxytocin mRNA Expression in BAT, Brain, Bone and Reproductive Tissue of Male Mice Using Real-Time PCR and Linear Correlation Analysis. Front Physiol 8, 1101. [PubMed: 29375393]

Cichon J, and Gan WB (2015). Branch-specific dendritic Ca(2+) spikes cause persistent synaptic plasticity. Nature 520, 180–185. [PubMed: 25822789]

Clements JD, Lester RA, Tong G, Jahr CE, and Westbrook GL (1992). The time course of glutamate in the synaptic cleft. Science 258, 1498–1501. [PubMed: 1359647]

Denes A, Boldogkoi Z, Uhereczky G, Hornyak A, Rusvai M, Palkovits M, and Kovacs KJ (2005). Central autonomic control of the bone marrow: multisynaptic tract tracing by recombinant pseudorabies virus. Neuroscience 134, 947–963. [PubMed: 15994021]

Di Somma C, Pivonello R, Loche S, Faggiano A, Klain M, Salvatore M, Lombardi G, and Colao A (2003). Effect of 2 years of cortisol normalization on the impaired bone mass and turnover in adolescent and adult patients with Cushing's disease: a prospective study. Clin Endocrinol (Oxf) 58, 302–308. [PubMed: 12608935]

Eiden LE (1998). The cholinergic gene locus. J Neurochem 70, 2227–2240. [PubMed: 9603187]

Fadok JP, Dickerson TM, and Palmiter RD (2009). Dopamine is necessary for cue-dependent fear conditioning. J Neurosci 29, 11089–11097. [PubMed: 19741115]

Ferron M, Wei J, Yoshizawa T, Del Fattore A, DePinho RA, Teti A, Ducy P, and Karsenty G (2010). Insulin signaling in osteoblasts integrates bone remodeling and energy metabolism. Cell 142, 296–308. [PubMed: 20655470]

Frankel AI, and Ryan EL (1981). Testicular innervation is necessary for the response of plasma testosterone levels to acute stress. Biol Reprod 24, 491–495. [PubMed: 7236815]

Furlan A, La Manno G, Lubke M, Haring M, Abdo H, Hochgerner H, Kupari J, Usoskin D, Airaksinen MS, Oliver G, et al. (2016). Visceral motor neuron diversity delineates a cellular basis for nipple- and pilo-erection muscle control. Nat Neurosci 19, 1331–1340. [PubMed: 27571008]

Haym I, Huynh TH, Hansen SW, Pedersen MH, Ruiz JA, Erichsen MN, Gynther M, Bjorn-Yoshimoto WE, Abrahamsen B, Bastlund JF, et al. (2016). Bioavailability Studies and in vitro Profiling of the Selective Excitatory Amino Acid Transporter Subtype 1 (EAAT1) Inhibitor UCPH-102. ChemMedChem 11, 403–419. [PubMed: 26797816]

Johansen JP, Cain CK, Ostroff LE, and LeDoux JE (2011). Molecular mechanisms of fear learning and memory. Cell 147, 509–524. [PubMed: 22036561]

Karsenty G, and Olson EN (2016). Bone and muscle endocrine functions: unexpected paradigms of inter-organ communication. Cell 164, 1248–1256. [PubMed: 26967290]

Khrimian L, Obri A, Ramos-Brossier M, Rousseaud A, Moriceau S, Nicot AS, Mera P, Kosmidis S, Karnavas T, Saudou F, et al. (2017). Gpr158 mediates osteocalcin's regulation of cognition. J Exp Med.

Kim J, Pignatelli M, Xu S, Itohara S, and Tonegawa S (2016). Antagonistic negative and positive neurons of the basolateral amygdala. Nat Neurosci 19, 1636–1646. [PubMed: 27749826]

Kobayakawa K, Kobayakawa R, Matsumoto H, Oka Y, Imai T, Ikawa M, Okabe M, Ikeda T, Itohara S, Kikusui T, et al. (2007). Innate versus learned odour processing in the mouse olfactory bulb. Nature 450, 503–508. [PubMed: 17989651]

Kondoh K, Lu Z, Ye X, Olson DP, Lowell BB, and Buck LB (2016). A specific area of olfactory cortex involved in stress hormone responses to predator odours. Nature.

Kusumbe AP, Ramasamy SK, Starsichova A, and Adams RH (2015). Sample preparation for high-resolution 3D confocal imaging of mouse skeletal tissue. Nat Protoc 10, 1904–1914. [PubMed: 26513669]

Lee NK, Sowa H, Hinoi E, Ferron M, Ahn JD, Confavreux C, Dacquin R, Mee PJ, McKee MD, Jung DY, et al. (2007). Endocrine regulation of energy metabolism by the skeleton. Cell 130, 456–469. [PubMed: 17693256]

Longo VG (1966). Behavioral and electroencephalographic effects of atropine and related compounds. Pharmacol Rev 18, 965–996. [PubMed: 5328390]

Mason DJ, Suva LJ, Genever PG, Patton AJ, Steuckle S, Hillam RA, and Skerry TM (1997). Mechanically regulated expression of a neural glutamate transporter in bone: a role for excitatory amino acids as osteotropic agents? Bone 20, 199–205. [PubMed: 9071469]

McEwen BS (1998). Protective and damaging effects of stress mediators. N Engl J Med 338, 171–179. [PubMed: 9428819]

Mera P, Laue K, Ferron M, Confavreux C, Wei J, Galan-Diez M, Lacampagne A, Mitchell SJ, Mattison JA, Chen Y, et al. (2016). Osteocalcin Signaling in Myofibers Is Necessary and Sufficient for Optimum Adaptation to Exercise. Cell Metab 23, 1078–1092. [PubMed: 27304508]

Mersebach H, Svendsen OL, Astrup A, and Feldt-Rasmussen U (2003). Abnormal sympathoadrenal activity, but normal energy expenditure in hypopituitarism. J Clin Endocrinol Metab 88, 5689–5695. [PubMed: 14671154]

Morrison NA, Shine J, Fragonas JC, Verkest V, McMenemy ML, and Eisman JA (1989). 1,25-dihydroxyvitamin D-responsive element and glucocorticoid repression in the osteocalcin gene. Science 246, 1158–1161. [PubMed: 2588000]

Muller M, and Fendt M (2006). Temporary inactivation of the medial and basolateral amygdala differentially affects TMT-induced fear behavior in rats. Behav Brain Res 167, 57–62. [PubMed: 16213603]

Orlandi C, Xie K, Masuho I, Fajardo-Serrano A, Lujan R, and Martemyanov KA (2015). Orphan Receptor GPR158 Is an Allosteric Modulator of RGS7 Catalytic Activity with an Essential Role in Dictating Its Expression and Localization in the Brain. J Biol Chem 290, 13622–13639. [PubMed: 25792749]

Oury F, Sumara G, Sumara O, Ferron M, Chang H, Smith CE, Hermo L, Suarez S, Roth BL, Ducy P, et al. (2011). Endocrine regulation of male fertility by the skeleton. Cell 144, 796–809. [PubMed: 21333348]

Patterson-Buckendahl P, Kvetnansky R, Fukuhara K, Cizza G, and Cann C (1995). Regulation of plasma osteocalcin by corticosterone and norepinephrine during restraint stress. Bone 17, 467–472. [PubMed: 8579958]

Pereira MM, Mahu I, Seixas E, Martinez-Sanchez N, Kubasova N, Pirzgalska RM, Cohen P, Dietrich MO, Lopez M, Bernardes GJ, et al. (2017). A brain-sparing diphtheria toxin for chemical genetic ablation of peripheral cell lineages. Nat Commun 8, 14967. [PubMed: 28367972]

Perry RJ, Peng L, Barry NA, Cline GW, Zhang D, Cardone RL, Petersen KF, Kibbey RG, Goodman AL, and Shulman GI (2016). Acetate mediates a microbiome-brain-beta-cell axis to promote metabolic syndrome. Nature 534, 213–217. [PubMed: 27279214]

Porges SW (1995). Cardiac vagal tone: a physiological index of stress. Neurosci Biobehav Rev 19, 225–233. [PubMed: 7630578]

Prather AA, Carroll JE, Fury JM, McDade KK, Ross D, and Marsland AL (2009). Gender differences in stimulated cytokine production following acute psychological stress. Brain Behav Immun 23, 622–628. [PubMed: 19070658]

Presnell SR, and Stafford DW (2002). The vitamin K-dependent carboxylase. Thromb Haemost 87, 937–946. [PubMed: 12083499]

Romer AS (1933). Eurypterid influence on vertebrate history. Science 78, 114–117. [PubMed: 17749819]

Root CM, Denny CA, Hen R, and Axel R (2014). The participation of cortical amygdala in innate, odour-driven behaviour. Nature 515, 269–273. [PubMed: 25383519]

Rost S, Fregin A, Ivaskevicius V, Conzelmann E, Hortnagel K, Pelz HJ, Lappegard K, Seifried E, Scharrer I, Tuddenham EG, et al. (2004). Mutations in VKORC1 cause warfarin resistance and multiple coagulation factor deficiency type 2. Nature 427, 537–541. [PubMed: 14765194]

Rothstein JD, Dykes-Hoberg M, Pardo CA, Bristol LA, Jin L, Kuncl RW, Kanai Y, Hediger MA, Wang Y, Schielke JP, et al. (1996). Knockout of glutamate transporters reveals a major role for astroglial transport in excitotoxicity and clearance of glutamate. Neuron 16, 675–686. [PubMed: 8785064]

Sapolsky RM, Romero LM, and Munck AU (2000). How do glucocorticoids influence stress responses? Integrating permissive, suppressive, stimulatory, and preparative actions. Endocr Rev 21, 55–89. [PubMed: 10696570]

Scimeca JC, Franchi A, Trojani C, Parrinello H, Grosgeorge J, Robert C, Jaillon O, Poirier C, Gaudray P, and Carle GF (2000). The gene encoding the mouse homologue of the human osteoclast-specific 116-kDa V-ATPase subunit bears a deletion in osteosclerotic (oc/oc) mutants. Bone 26, 207–213. [PubMed: 10709991]

Serre CM, Farlay D, Delmas PD, and Chenu C (1999). Evidence for a dense and intimate innervation of the bone tissue, including glutamate-containing fibers. Bone 25, 623–629. [PubMed: 10593406]

Skerry T, Genever P, Taylor A, Dobson K, Mason D, and Suva L (2001). Absence of evidence is not evidence of absence. The shortcomings of the GLAST knockout mouse. J Bone Miner Res 16, 1729–1730; author reply 1731-1722. [PubMed: 11547846]

Takeda S, Elefteriou F, Levasseur R, Liu X, Zhao L, Parker KL, Armstrong D, Ducy P, and Karsenty G (2002). Leptin regulates bone formation via the sympathetic nervous system. Cell 111, 305–317. [PubMed: 12419242]

Talman WT, Perrone MH, and Reis DJ (1980). Evidence for L-glutamate as the neurotransmitter of baroreceptor afferent nerve fibers. Science 209, 813–815. [PubMed: 6105709]

Terburg D, Scheggia D, Triana Del Rio R, Klumpers F, Ciobanu AC, Morgan B, Montoya ER, Bos PA, Giobellina G, van den Burg EH, et al. (2018). The Basolateral Amygdala Is Essential for Rapid Escape: A Human and Rodent Study. Cell 175, 723–735 e716. [PubMed: 30340041]

Tie JK, Jin DY, Loiselle DR, Pope RM, Straight DL, and Stafford DW (2004). Chemical modification of cysteine residues is a misleading indicator of their status as active site residues in the vitamin K-dependent gamma-glutamyl carboxylation reaction. J Biol Chem 279, 54079–54087. [PubMed: 15492002]

Toyota M, Spencer D, Sawai-Toyota S, Jiaqi W, Zhang T, Koo AJ, Howe GA, and Gilroy S (2018). Glutamate triggers long-distance, calcium-based plant defense signaling. Science 361, 1112–1115. [PubMed: 30213912]

Tsai MJ, and O'Malley BW (1994). Molecular mechanisms of action of steroid/thyroid receptor superfamily members. Annu Rev Biochem 63, 451–486. [PubMed: 7979245]

Tye KM, Prakash R, Kim SY, Fenno LE, Grosenick L, Zarabi H, Thompson KR, Gradinaru V, Ramakrishnan C, and Deisseroth K (2011). Amygdala circuitry mediating reversible and bidirectional control of anxiety. Nature 471, 358–362. [PubMed: 21389985]

Ulrich-Lai YM, and Herman JP (2009). Neural regulation of endocrine and autonomic stress responses. Nat Rev Neurosci 10, 397–409. [PubMed: 19469025]

Viviani D, Charlet A, van den Burg E, Robinet C, Hurni N, Abatis M, Magara F, and Stoop R (2011). Oxytocin selectively gates fear responses through distinct outputs from the central amygdala. Science 333, 104–107. [PubMed: 21719680]

Vizi ES (1973). Acetylcholine release from guinea-pig ileum by parasympathetic ganglion stimulants and gastrin-like polypeptides. Br J Pharmacol 47, 765–777. [PubMed: 4723798]

Vong L, Ye C, Yang Z, Choi B, Chua S Jr., and Lowell BB (2011). Leptin action on GABAergic neurons prevents obesity and reduces inhibitory tone to POMC neurons. Neuron 71, 142–154. [PubMed: 21745644]

Watkins JC, and Jane DE (2006). The glutamate story. Br J Pharmacol 147 Suppl 1, S100–108. [PubMed: 16402093]

Wei J, Shimazu J, Makinistoglu MP, Maurizi A, Kajimura D, Zong H, Takarada T, Iezaki T, Pessin JE, Hinoi E, et al. (2015). Glucose Uptake and Runx2 Synergize to Orchestrate Osteoblast Differentiation and Bone Formation. Cell 161, 1576–1591. [PubMed: 26091038]

Weigand LA, Kwong K, and Myers AC (2015). The Effects of Nerve Growth Factor on Nicotinic Synaptic Transmission in Mouse Airway Parasympathetic Neurons. Am J Respir Cell Mol Biol 53, 443–449. [PubMed: 25647301]

Wolff SB, Grundemann J, Tovote P, Krabbe S, Jacobson GA, Muller C, Herry C, Ehrlich I, Friedrich RW, Letzkus JJ, et al. (2014). Amygdala interneuron subtypes control fear learning through disinhibition. Nature 509, 453–458. [PubMed: 24814341]

Xing L, Salas M, Zhang H, Gittler J, Ludwig T, Lin CS, Murty VV, Silverman W, Arancio O, and Tycko B (2013). Creation and characterization of BAC-transgenic mice with physiological overexpression of epitope-tagged RCAN1 (DSCR1). Mamm Genome 24, 30–43. [PubMed: 23096997]

Yadav VK, Ryu JH, Suda N, Tanaka KF, Gingrich JA, Schutz G, Glorieux FH, Chiang CY, Zajac JD, Insogna KL, et al. (2008). Lrp5 controls bone formation by inhibiting serotonin synthesis in the duodenum. Cell 135, 825–837. [PubMed: 19041748]

Yoshikawa Y, Kode A, Xu L, Mosialou I, Silva BC, Ferron M, Clemens TL, Economides AN, and Kousteni S (2011). Genetic evidence points to an osteocalcin-independent influence of osteoblasts on energy metabolism. J Bone Miner Res 26, 2012–2025. [PubMed: 21557308]

Yuen EY, Liu W, Karatsoreos IN, Feng J, McEwen BS, and Yan Z (2009). Acute stress enhances glutamatergic transmission in prefrontal cortex and facilitates working memory. Proc Natl Acad Sci U S A 106, 14075–14079. [PubMed: 19666502]

Zhu H, and Roth BL (2014). Silencing synapses with DREADDs. Neuron 82, 723–725. [PubMed: 24853931]

Zuckerman-Levin N, Tiosano D, Eisenhofer G, Bornstein S, and Hochberg Z (2001). The importance of adrenocortical glucocorticoids for adrenomedullary and physiological response to stress: a study in isolated glucocorticoid deficiency. J Clin Endocrinol Metab 86, 5920–5924. [PubMed: 11739465]

Highlights

- The acute stress response (ASR) stimulates osteocalcin release from bone within minutes
- Glutamate uptake into osteoblasts is required for osteocalcin release during an ASR
- Osteocalcin inhibits the parasympathetic tone during an ASR
- In adrenal insufficiency, increased osteocalcin levels enable an ASR to occur

Context and Significance

A major question in skeletal biology is to understand why bone, through the hormone osteocalcin, favors energy metabolism, reproduction, memory and the ability to exercise. Since most of these functions abet survival in unpredictably hostile environments like the wild, we surmised that bone evolved to enable vertebrates to overcome acute danger. In support of this notion, this study shows that animals need osteocalcin to develop an acute stress response, a function critical to survival in the wild. When animals encounter an immediate danger, a brain-derived signal stimulates the release of osteocalcin from bone. Once released, osteocalcin turns off the parasympathetic or “rest-and-digest” arm of the autonomic nervous system and thereby allows the acute stress response to proceed.

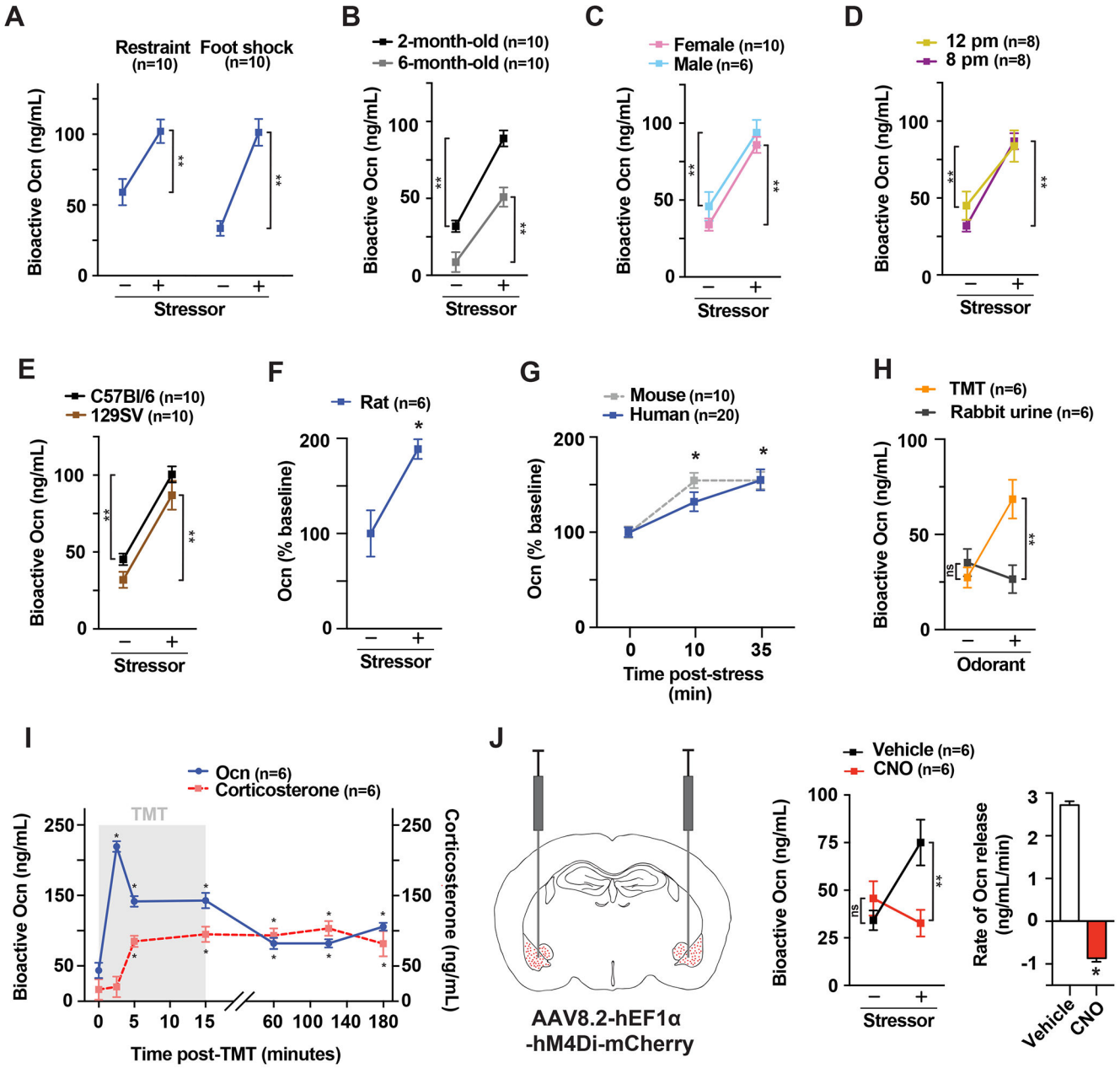

Figure 1. Stressors trigger a rapid surge of circulating bioactive osteocalcin (Ocn) in rodents and humans.

(A) Serum Ocn levels in 3-month-old WT mice after restraint or foot shocks. **(B-E)** Serum Ocn levels in 2- and 6-month-old, male and female WT mice, at 12 p.m. and 8 p.m., and C57Bl/6 or 129SV WT mice after foot shocks. **(F)** Serum Ocn levels in WT female rats after restraint. **(G)** Serum Ocn levels in WT mice after foot shock and humans after public speaking stress. **(H)** Serum Ocn levels in WT mice after TMT or rabbit urine exposure. **(I)** Serum Ocn and corticosterone levels in TMT-exposed WT mice (gray). **(J)** Serum Ocn levels and rate of Ocn release in TMT-exposed WT mice expressing *hM4Di* in the BLA after injection of CNO or vehicle. Mice are 3-month-old females unless otherwise specified.

Values are mean ±SEM. ns, not significant; *, p<.05; **, p<.01; by Student's t-test or one-way ANOVA with Bonferroni post hoc test.

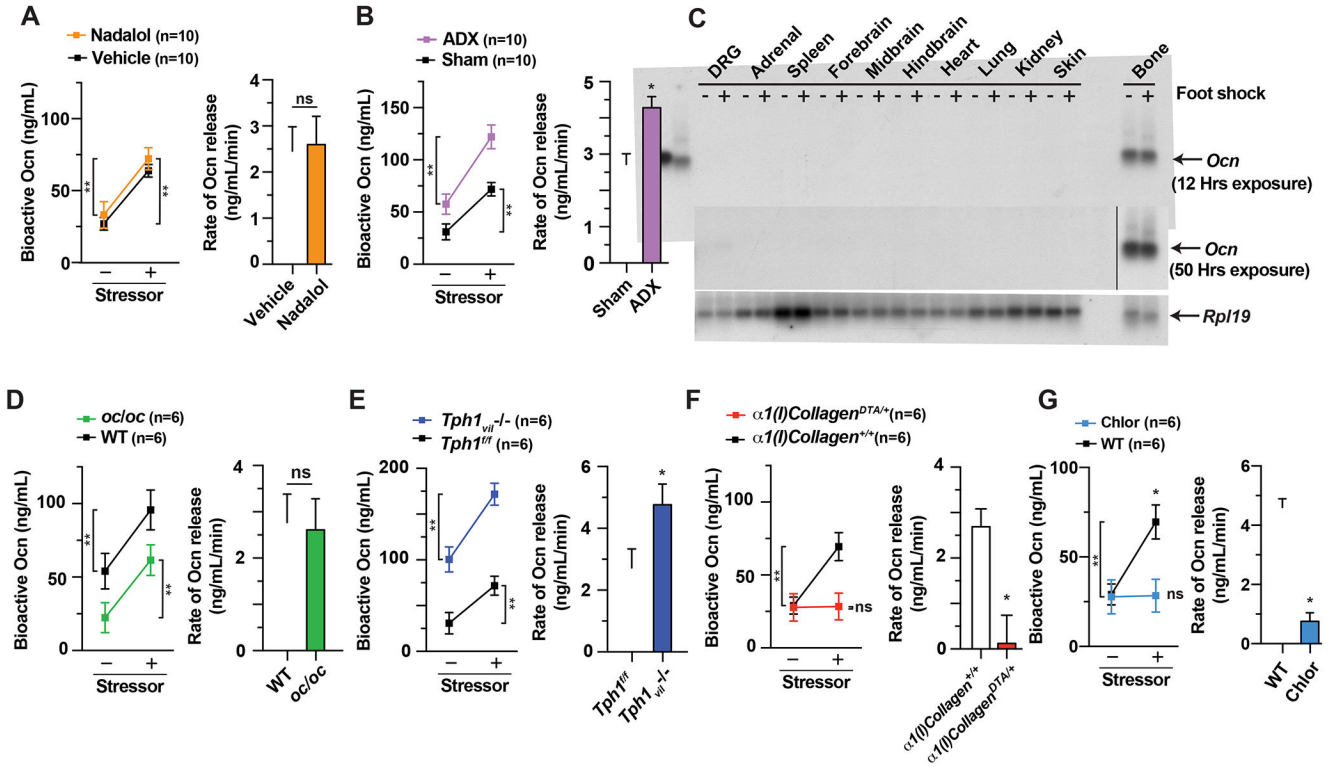

Figure 2. Bioactive osteocalcin is released from cells of the osteoblast lineage during an acute stress response.

(A) Serum Ocn levels and rate of Ocn release in nadolol- and vehicle-treated WT mice exposed to TMT. **(B)** Serum Ocn levels and rate of Ocn release in adrenalectomized (ADX) and sham-operated TMT-exposed WT mice. **(C)** Northern blot analysis of *Ocn* (top) and *L19* (bottom) expression after foot shock. **(D)** Serum Ocn levels and rate of Ocn release in *oc/oc* and WT mice before and after TMT exposure. **(E)** Serum Ocn levels and rate of Ocn release in Tph_{vil}−/− and $Tph^{f/f}$ mice before and after TMT exposure. **(F)** Serum Ocn levels and rate of Ocn release in $\alpha 1(I)\ Collagen^{DTA/+}$ and $\mu 1(I)\ Collagen^{+/+}$ mice before and after TMT exposure. **(G)** Serum Ocn levels and rate of Ocn release in chlorisondamine- and vehicle-treated WT mice before and after TMT exposure. Mice are 3-month-old females. Rats are 4-month-old females. Values are mean ±SEM. ns, not significant; *, p<.05; **, p<.01; by Student's t- test or one-way ANOVA with Bonferroni post hoc test.

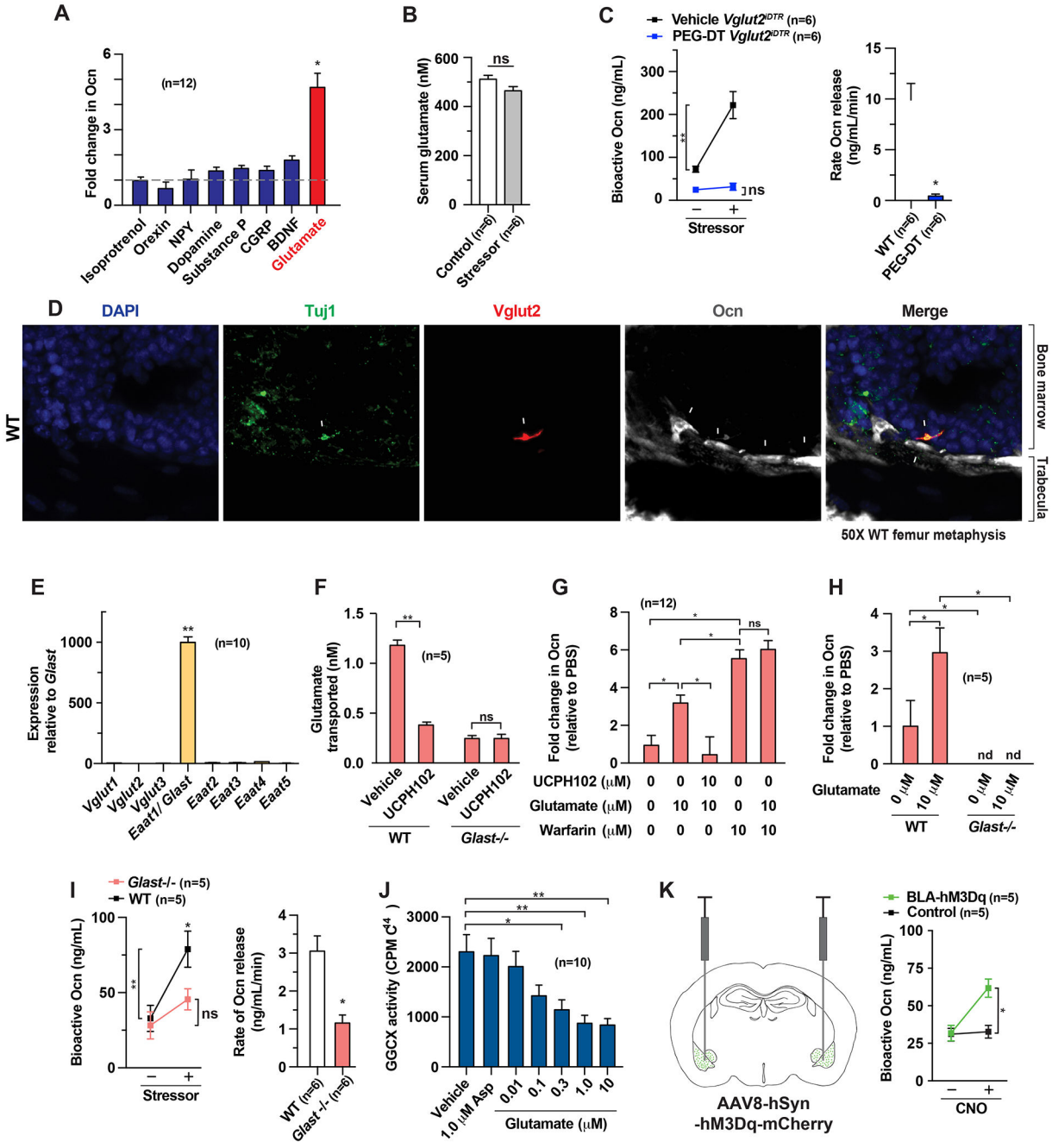

Figure 3. Glutamate mediates the stressor-induced release of bioactive osteocalcin from osteoblasts.

(A) Supernatant Ocn levels after 1-hour treatment of osteoblasts with indicated neurotransmitters. **(B)** Serum glutamate levels before and after TMT exposure. **(C)** Serum Ocn levels and rate of Ocn release before and after TMT stress in pegylated diphtheria toxin (PEG-DT)- or vehicle-injected *Vglut2*^{iDTR} mice. **(D)** Immunofluorescence of femoral metaphysis of WT mice, Ob: osteoblast, N: glutamatergic neurite (scale: 5 μm). **(E)** Expression of glutamate transporters in osteoblasts. **(F)** Radiolabeled glutamate transport into *Glast*−/− and WT osteoblasts treated with vehicle or UCPH102. **(G)** Ocn levels in

supernatants after 1-hour treatment with glutamate and UCPH102 of untreated or warfarin pre-treated mouse osteoblast cultures. **(H)** Supernatant Ocn levels 1 hour after treatment of *Glast*−/− and WT osteoblasts with glutamate. **(I)** Serum Ocn levels and rate of Ocn release in *Glast*−/− and WT mice before and after TMT exposure. **(J)** GGCX activity on Ocn in WT osteoblast lysates treated with glutamate. **(K)** Serum Ocn in WT mice expressing *hM3Dq* in the BLA after injection of CNO or vehicle. Mice are 3-month-old females. Values are mean ±SEM. nd, not detectible. ns, not significant; *, p<.05; **, p<.01; by Student's t-test or one-way ANOVA with bonferroni post hoc test.

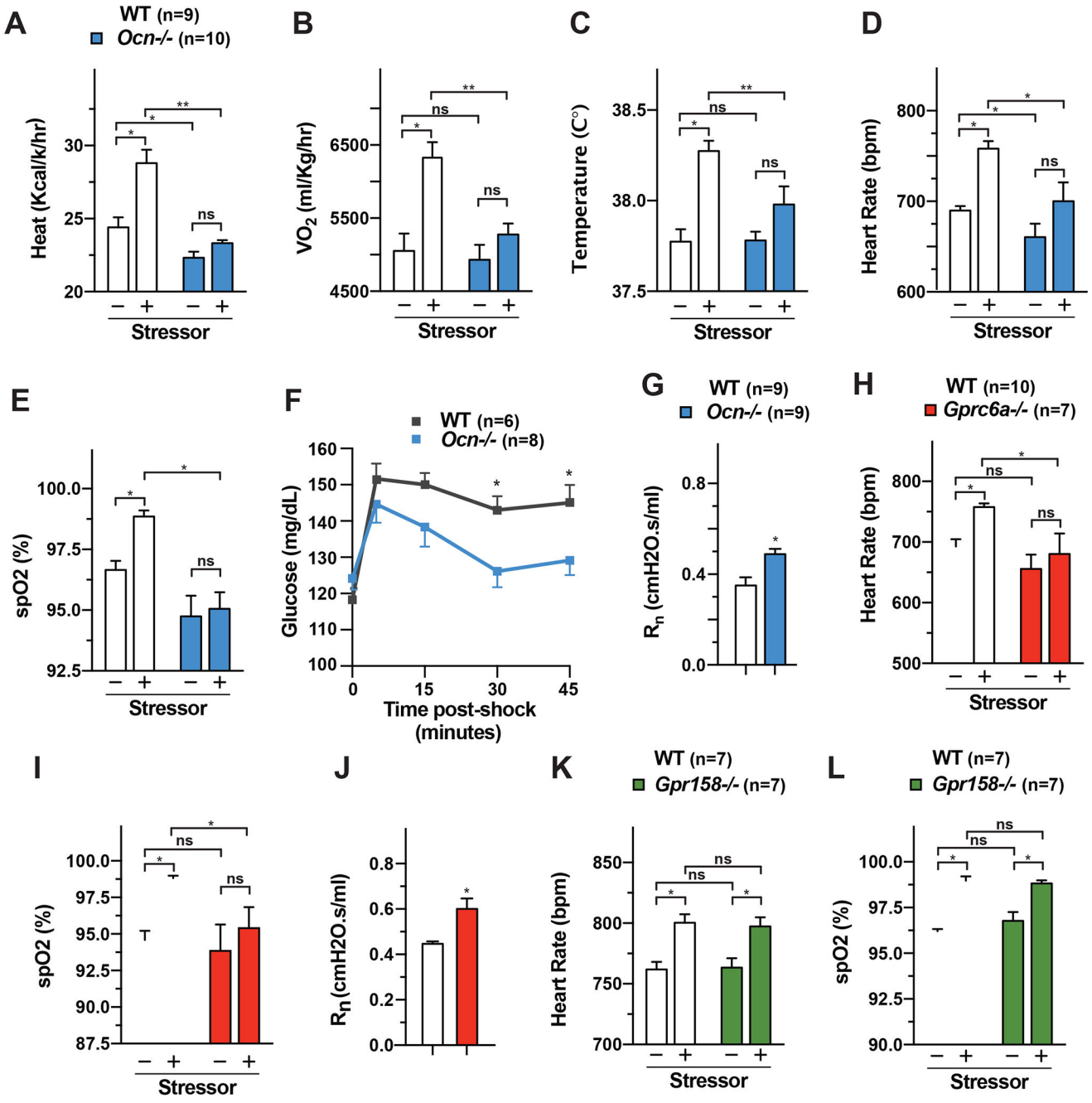

Figure 4. Osteocalcin signaling in peripheral organs is necessary to mount an ASR.

(A-F) Energy expenditure, oxygen consumption, temperature, heart rate, arterial oxygen saturation and blood glucose in *Ocn*−/− and WT mice before and after foot shock. **(G)** Newtonian airway resistance in *Ocn*−/− and WT mice. **(H-I)** Heart rate and arterial oxygen saturation in *Gprc6a*−/− and WT mice before and after foot shock. **(J)** Newtonian airway resistance in *Gprc6a*−/− and WT mice. **(K-L)** Heart rate and arterial oxygen saturation in *Gpr158*−/− and WT mice before and after foot shock. Mice are 3-month-old females. Rats are 4-month-old females. Values are mean ±SEM. ns, not significant; *, p<.05; **, p<.01; by Student's t-test or one-way ANOVA with bonferroni post hoc test.

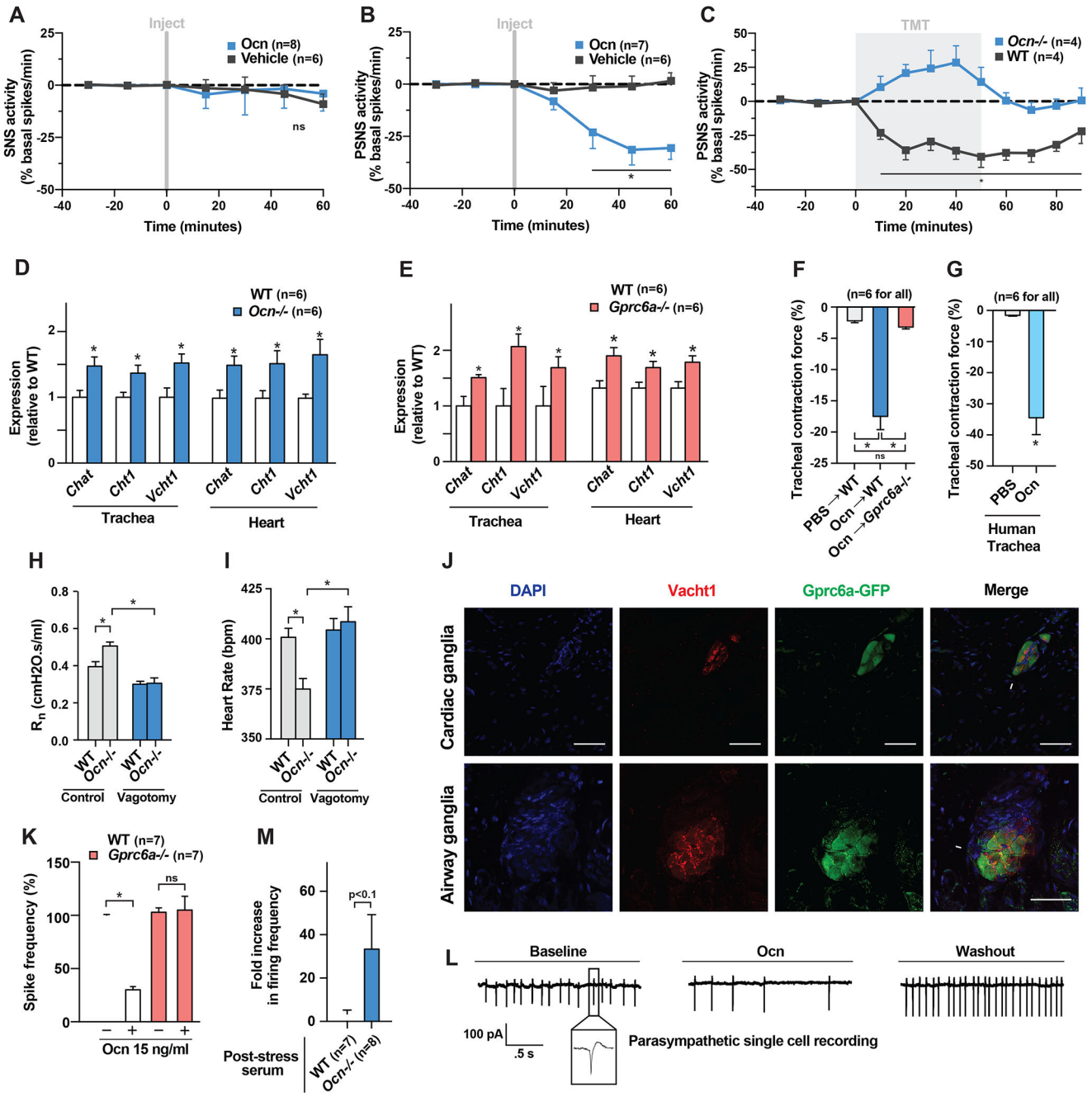

Figure 5. Osteocalcin inhibits parasympathetic tone during an ASR.

(A) Sympathetic nerve activity in WT mice injected with Ocn (30 ng/g) or vehicle. **(B)** Parasympathetic nerve activity in WT mice injected with Ocn (30 ng/g) or vehicle. **(C)** Parasympathetic nerve activity after TMT exposure in *Ocn*−/− and WT littermates. **(D-E)** *Chat*, *Cht1* and *Vachtl* expression in trachea and heart of *Ocn*−/−, Gprc6a−/− and WT littermates. **(F)** Contraction of electrically stimulated *Gprc6a*−/− or WT mouse tracheal rings treated with Ocn (10 ng/ml) or vehicle. **(G)** Contraction of electrically stimulated human tracheal rings treated with Ocn (10 ng/ml) or vehicle. **(H-I)** Newtonian airway resistance and heart rate in vagotomized or sham-operated *Ocn*−/− and WT mice. **(J)** Immunofluorescence

of airway (scale bar: 15 μm) and cardiac ganglia of *Gprc6a-Gfp* mice, PG: parasympathetic ganglia (scale bar: 12 μm). **(K-L)** Firing frequency in WT and *Gprc6a*−/− tracheal post-ganglionic parasympathetic neurons before, during and after treatment with Ocn (15 ng/ml) normalized to control and representative traces of action currents in *Ocn*−/− or vehicle-treated WT tracheal post-ganglionic parasympathetic neurons. **(M)** Firing frequency in tracheal post-ganglionic parasympathetic neurons after treatment with sera from stressed *Ocn*−/− or WT mice. Mice are 3-month-old females. Values are mean ±SEM. ns, not significant; *, p<.05; **, p<.01; by Student's t-test or one-way ANOVA with bonferroni post hoc test.

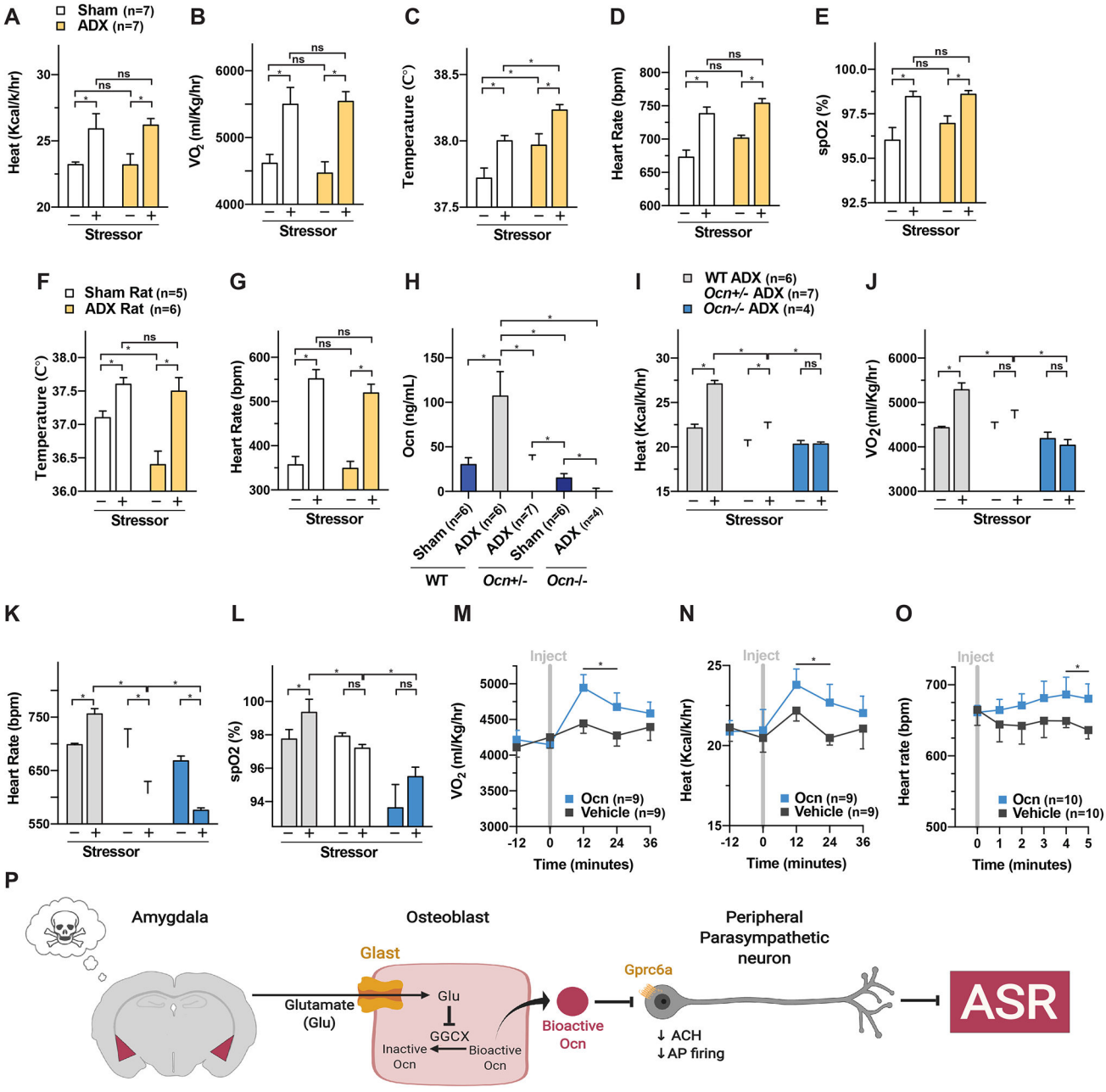

Figure 6. High circulating osteocalcin levels account for the ability of adrenalectomized mice to develop an ASR.

(A-E) Energy expenditure, oxygen consumption, temperature, heart rate and arterial oxygen saturation in ADX and sham-operated mice before and after foot shock. **(F-G)** Temperature and heart rate in ADX and sham-operated rats before and after restraint. **(H)** Serum Ocn levels in WT sham-operated, ADX, *Ocn*+/− ADX, *Ocn*+/− sham-operated and *Ocn*−/− ADX mice. **(I-J)** Energy expenditure and oxygen consumption in WT ADX, *Ocn*+/− ADX and *Ocn*−/− ADX mice before and after foot shock. **(K-L)** Heart rate and arterial oxygen saturation in WT ADX, *Ocn*+/− ADX and *Ocn*−/− ADX mice before and after foot shock. **(M-O)** Energy expenditure, oxygen consumption and heart rate in WT mice injected with

Ocn (30 ng/g) or vehicle. **(P)** Schematic representation of the endocrine mediation of the ASR in bony vertebrates. Stress signaling in the amygdala results in glutamate release in bone. Glutamate enters osteoblasts through Glast, exerts a competitive inhibition on GGCX and as a result bioactive Ocn is released. Ocn binds to Gprc6a on peripheral parasympathetic neurons to inhibit their activity, allowing the ASR to begin (AP, action potential). Mice are 3-month-old females. Rats are 4-month-old females. Values are mean ±SEM. ns, not significant; *, $p<.05$; **, $p<.01$; by Student's t-test or one-way ANOVA with bonferroni post hoc test.

KEY RESOURCES TABLE

REAGENT or RESOURCE	SOURCE	IDENTIFIER
Antibodies		
anti-Vglut2	Synaptic Systems	135403
anti-III Tubulin	Abcam	2G10
anti-GFP	Abcam	ab13970
anti-Vacht1 (Millipore: ABN100	Millipore	ABN100
anti-Beta galactosidase	Abcam	ab4761
anti-MCherry	Abcam	ab167453
anti-a-tubulin	Sigma	T6199
anti-RankL	abcam	ab45039
Anti-Type I collagen	Rockland Inc.	600-401-103-0.5
Bacterial and Virus Strains		
AAV8.2-hEF1α-hM4Di-mCherry-WPRE	MIT Viral gene Transfer Core	N/A
pGEX2TK-mOCN	Lee et al., 2007	N/A
Chemicals, Peptides, and Recombinant Proteins		
Collagenase Type 4	Worthington	LS004188
Ascorbic Acid	Sigma	PHR1008
alpha-tocopherol	Sigma	258024
insulin	Sigma	I9278
2,3,5-Trimethyl-3-thiazoline (TMT)	Scotts Canada Ltd	300000368
nadalol	Sigma	N1892
Alendronate sodium	Sigma	1012780
tamoxifen	Sigma	T5648
phosphatase inhibitor cocktail	Thermo	78443
glutathione-sepharose	GE	17075601
thrombin	GE	27-0846-01
Benzamidine sepharose	GE	17-5123-10
ACTH	Phoenix Pharmaceuticals	001-21
Pituitary extract	Thermofisher	13028014
Growth hormone	Biovision	4770
TSH	Sigma	T8193
LH	Sigma	L5269
FSH	Sigma	F2293
Prolactin	Sigma	SRP4688
MSH	Sigma	M4135
PTH	Sigma	P3921
Leptin	Sigma	L3772
Insulin	Sigma	I3536

REAGENT or RESOURCE	SOURCE	IDENTIFIER
Glucagon	Sigma	G2044
Dexamethasone	Sigma	D4902
Isoproterenol	Sigma	1351005
Orexin A	Phoenix Pharmaceuticals	003-30
NPY	BACHEM	H-6375
Dopamine	Sigma	H8502
substance P	Sigma	S6883
CGRP	Phoenix Pharmaceuticals	15-09
BDNF	Peprotech	450-02
Glutamate	Sigma	49621
UCPH-102	abcam	146404
Atropine	Sigma	A0132
clozapine-N-oxide (CNO)	Sigma	C0832
Critical Commercial Assays		
CTX ELISA	IDS	AC-02F1
Corticosterone ELISA	abcam	ab108821
ACTH ELISA	MDBioscience	M046006s
PiNP ELISA	IDS	AC-33F1
Gastrin ELISA	Sigma	RAB0200
Glutamate ELISA	Abcam	ab83389
Sclerostin ELISA	R and D	MSST00
Fgf23 ELISA	Kainos	CY-4000
Gla-OCN ELISA	Takara	MK111
Total OCN ELISA	Alpco	38-OSTHU-E01
Experimental Models: Organisms/Strains		
Ocn−/− (*osc*^{m1}/*osc*^{m1}) mice	Ducy et al., 1996	RRID:MGI:3763089
Gpr158$^{tm1.1(KOMP)Vlcg}$	KOMP repository	RRID:MGI:5887391
Gprc6a−/−	Oury et al., 2011	RRID:MGI:2174761
Oc/oc mice	Dr. Anna Villa, IRGB, Italy	RRID:MGI:2174761
Tph1$_{vil}^{fl/fl}$ mice	Yadav et al., 2008	RRID:MGI:3837407
Gprc6a-gfp mice	This paper	N/A
Glast−/− mice	This paper	N/A
C57BL/6J mice	The Jackson Laboratory	RRID:IMSR_JAX:000664
129S6/SvEvTac	Taconic Biosciences	**RRID:IMSR_TAC:129sve**
DTA mice	Dr. Stavroula Kousteni, Columbia University (Yoshikawa et al., 2011)	RRID:MGI:5514395
B6.Cg-Tg(Col1a1-cre/ERT2)1Crm/J	The Jackson Laboratory	RRID:IMSR_JAX:016241
Software and Algorithms		
FIJI ImageJ	NIH	https://imagej.net/Fiji/Downloads

REAGENT or RESOURCE	SOURCE	IDENTIFIER
Prism	Graphpad Software	https://www.graphpad.com/scientific-software/prism/
Acqknowledge software	BioPac Systems	https://www.biopac.com/product/acqknowledge-software/
Other		
Columbus Instruments	Columbus Instruments	
Conditioning apparatus	MedAssociates, USA	
Mouse OX	Starr Life Sciences	
Flexivent	Scireq, Ca	N/A
Element POC	Heska	N/A
Hamilton syringe	Hamilton	N/A
Warfarin	Santa Cruz	65458-01
AAV8-hSyn-hM3Dq-mCherry-WPRE	Addgene	129066
anti-VGLUT2	Abcam	50474-AAV8
anti- TH	Millipore	ab29157
anti-NF200	Millipore	ab1542
IB4 isolectin	Thermofisher	ab5539
anti-PVALB	Swant	I23450
anti-PGP9.5	Millipore	PVG-213
anti-CGRP	SIgma	ab5925
anti-TH	Cell Signaling	C8198
anti-Phospho-CREB	Cell Signaling	2792
anti-CREB	Cell Signaling	9198
Anti-GAPDH	Cell Signaling	D16H11